Received: 23 March 2022 | Revised: 16 August 2022 | Accepted: 25 August 2022

DOI: 10.1111/bre.12715

Basin Research | IAS EAGE | WILEY

RESEARCH ARTICLE

Reorganization of continent-scale sediment routing based on detrital zircon and rutile multi-proxy analysis

Maximilian Dröllner | **Milo Barham** | **Christopher L. Kirkland**

Timescales of Mineral Systems Group, The Institute of Geoscience Research, School of Earth and Planetary Sciences, Curtin University, Perth, Western Australia, Australia

Correspondence
Maximilian Dröllner, Timescales of Mineral Systems Group, The Institute of Geoscience Research, School of Earth and Planetary Sciences, Curtin University, GPO Box U1987, Perth, WA 6845, Australia.
Email: maximilian.droellner@postgrad.curtin.edu.au

Funding information
Australian Research Council LIEF programme, Grant/Award Number: LE150100013; The Institute for Geoscience Research; MRIWA, Grant/Award Number: M551

Abstract

The duration and extent of sediment routing systems are intrinsically linked to crustal- to mantle-scale processes. Therefore, distinct changes in the geodynamic regime may be captured in the detrital record. This study attempts to reconstruct the sediment routing system of the Canning Basin (Western Australia) during the Early Cretaceous to decipher its depositional response to Mesozoic-Cenozoic supercontinent dispersal. Specifically, we reconstruct source-to-sink relationships for the Broome Sandstone (Dampier Peninsula) and proximal modern sediments through multi-proxy analysis of detrital zircon (U–Pb, Lu–Hf and trace elements) and detrital rutile (U–Pb and trace elements). Multi-proxy comparison of detrital signatures and potential sources reveals that the majority of the detrital zircon and rutile grains are ultimately sourced from crystalline basement in central Australia (Musgrave Province and Arunta region) and that proximal sediment supply (i.e., Kimberley region) is negligible. However, a significant proportion of detritus might be derived from intermediate sedimentary sources in central Australia (e.g., Amadeus Basin) rather than directly from erosion of crystalline basement. Broome Sandstone data are consistent with a large-scale drainage system with headwaters in central Australia. Contextualization with other broadly coeval drainage systems suggests that central Australia acted as a major drainage divide during the Early Cretaceous. Importantly, reorganization after supercontinent dispersal is characterized by the continuation of a sediment pathway remnant of an earlier transcontinental routing system originating in Antarctica that provided a template for Early Cretaceous drainage. Review of older Canning Basin strata implies a prolonged denudation history of central Australian lithologies. These observations are consistent with the long-lived intracontinental tectonic activity of central Australia governing punctuated sediment generation and dispersion more broadly across Australia and emphasize the impact of deep Earth processes on sediment routing systems.

KEYWORDS

detrital rutile, Hf isotopes, provenance, sediment routing, source to sink, trace elements, U–Pb geochronology

1 | INTRODUCTION

Sediment generation and transport pathways are extrinsically governed by tectonic and climatic processes (e.g., Armitage et al., 2011; Blum et al., 2018). Thus, crustal- to mantle-scale processes, such as tectonic deformation (e.g., Castelltort et al., 2012; Clark et al., 2004; Olierook et al., 2019), mantle hotspots (Chardon et al., 2016) and mantle convection (Faccenna et al., 2019) are first-order controls of erosional activity and the spatiotemporal evolution of drainage patterns. These external factors may control lifespans of sediment pathways that can persist for several 100 s of Myr (e.g., Morón et al., 2019; Prokopiev et al., 2008), but can also drive significant reorganization or fragmentation of sediment routing systems over different timescales and can leave characteristic imprints on the detrital record (e.g., Barham & Kirkland, 2020; Blum & Pecha, 2014; Song et al., 2022; Tyrrell et al., 2007). Therefore, studying variations of sedimentary compositions within basins can inform the co-evolution of drainage pattern and their controls (e.g., Davis et al., 2010; Zhang et al., 2019).

Palaeozoic–Mesozoic sedimentary successions of the Canning Basin (Western Australia), have been interpreted to form a section of an ancient transcontinental drainage system of East Gondwana with headwaters in Antarctica (Morón et al., 2019; Figure 1a). Importantly, the stratigraphy preserved within the basin is an almost continuous record of the drainage evolution of East Gondwana and provides an opportunity to study the reorganization of continental sediment routing systems after Mesozoic-Cenozoic supercontinent dispersal. The sediment pathways of Palaeozoic and lower Mesozoic sedimentary rocks of the Canning Basin and the equivalent offshore Carnarvon Basin, which accumulated prior to the separation of Antarctica and Greater India from Australia, have been interpreted from U–Pb and Hf isotope analysis of detrital zircon (e.g., Haines et al., 2013; Haines & Wingate, 2007; Morón et al., 2019; Zutterkirch et al., 2021).

The breakup of East Gondwana commenced with seafloor spreading northwest of Australia at ca. 136 Ma, which propagated southward and separated Greater India and Australia-Antarctica at ca. 126 Ma (Gibbons et al., 2013). Although the breakup of Antarctica and southwestern Australia is constrained at ca. 90 Ma based on the onset of seafloor spreading (Direen, 2011), the fluvial connection between the continents was likely terminated significantly earlier. Arguably, sediment transport from Antarctica to Australia ceased with the crustal thinning and extension that was initiated during the Late Jurassic (Sayers et al., 2001). This is supported by (i) absence of Antarctica-derived detritus in the Early Cretaceous Madura Shelf in southern Australia (Barham et al., 2018) and (ii) paleodrainage patterns of south-western Australia that are consistent with paleocurrent direction towards Antarctica (see figure 3 in Olierook et al., 2015) and have minimum depositional ages of ca. 137 Ma (based on ^{40}Ar-^{39}Ar ages of overlying lava flows; Olierook et al., 2016), suggesting no effective fluvial sediment transport from Antarctica to Australia during the Early Cretaceous. However, a detailed model on the sediment routing system of the Canning Basin after the separation of Greater India, and during and after the initiation of rifting with Antarctica is currently lacking, hampering the study of sedimentary reorganization after these major geodynamic changes.

Reconstructing sediment transport pathways using detrital zircon crystallization ages as distinctive tracers may be hindered in cases where potential source rocks share similar age characteristics, obscuring definitive source-to-sink interpretations (e.g., Howard et al., 2009; Xu et al., 2017). Hence, a robust source discrimination, capable of disentangling various non-distinctive source signals, demands a multi-proxy approach. Lu–Hf isotope geochemistry, sensitive to the source of the melt in which the zircon crystallized, has been utilized to improve the interpretation of sediment source terranes (e.g., Barham & Kirkland, 2020; Ustaömer et al., 2016; Veevers et al., 2005). The ^{176}Hf/^{177}Hf ratio that is commonly expressed using the epsilon notation (εHf; deviation from the chondritic Hf ratio), can inform about the tectonic setting of zircon formation (e.g., Belousova et al., 2010; Collins et al., 2011). Thus, sources of near-contemporaneous formation but distinct tectonic setting can be distinguished based on their Hf isotopic fingerprint, for example, zircon from arc settings show more radiogenic (juvenile) compositions (+ εHf) than zircon in continent-collision settings that show less radiogenic (more evolved) Hf signals (− εHf) (e.g., Gardiner et al., 2016). Additional provenance information

HIGHLIGHTS

- Multi-proxy analysis of the detrital record captures sedimentary reorganization after major geodynamic changes.
- Integration of U-Pb, Hf isotope and trace element analyses of detrital zircon and rutile improve discrimination of potential source areas of broadly coeval age.
- Source-to-sink correlation is consistent with an Early Cretaceous sediment routing system with headwaters in central Australia.
- Pre-existing Gondwanan sediment pathways provided a template for Early Cretaceous drainage.

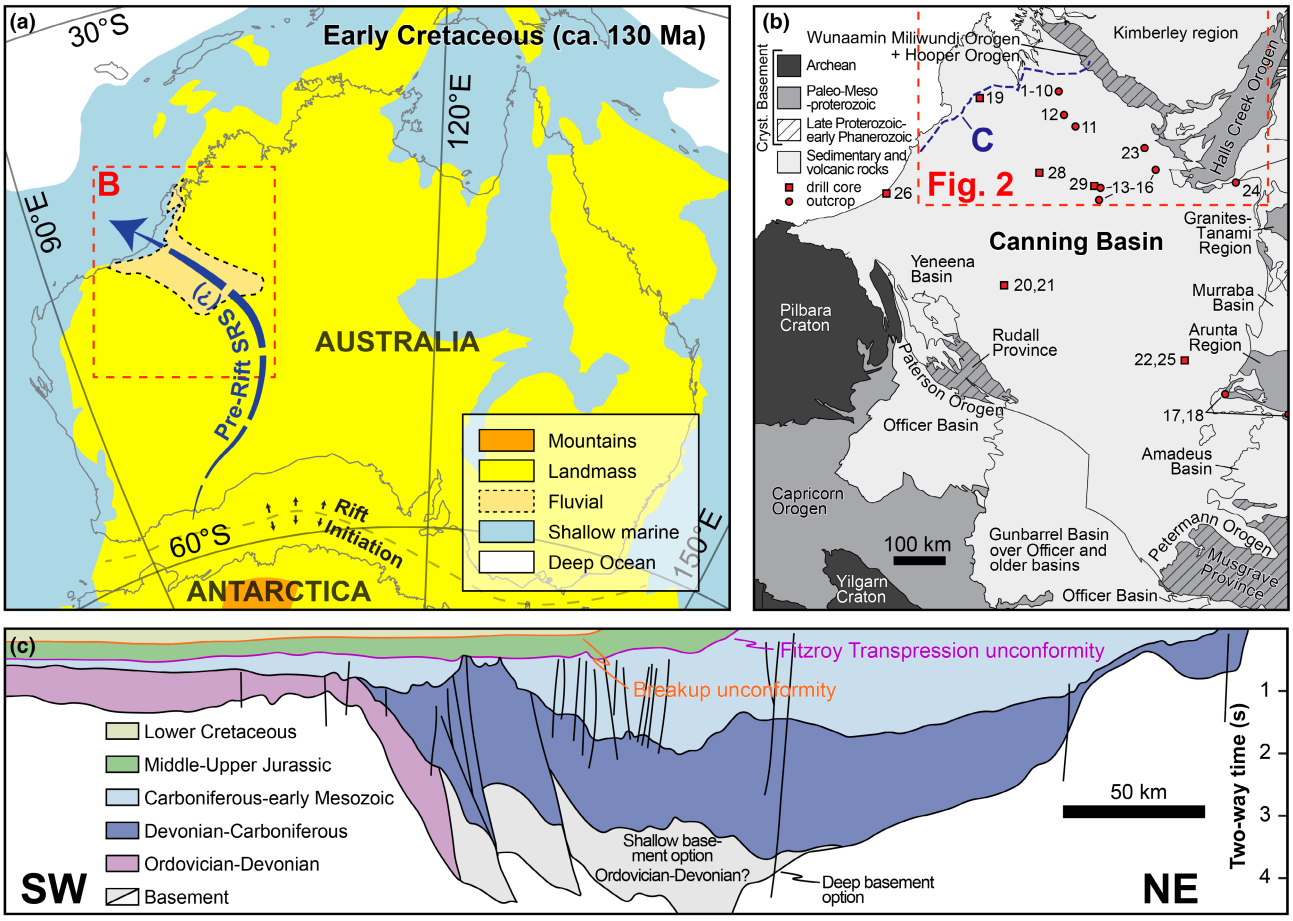

FIGURE 1 (a) Paleogeographic reconstruction of Australia during the early cretaceous (ca. 130 Ma); modified after Totterdell et al. (2001) and Cao et al. (2017) using the GPlates 2.3 software (Müller et al., 2018). Pale grey lines define modern coastlines. Red dashed line shows the extent of (b). SRS, Sediment routing system. (b) Simplified map of major geological units bordering the Canning Basin (modified after Haines et al., 2013). Red dots and squares show locations of reference samples (outcrop and drill core, respectively) used in Figure 9. Red dashed line shows the extent of Figure 2. Blue line labelled 'C' shows the approximate course of seismic profile in (c). (c) Simplified interpretation of a seismic cross-section of the north-eastern part of the Canning Basin (modified after Hashimoto et al., 2018).

may be retrieved by the integrated measurements of trace element compositions of detrital minerals, which inform about source rock petrology (e.g., Belousova et al., 2002; Grimes et al., 2007; Hoskin & Ireland, 2000). Trace elements can address various source rock characteristics, for example the tectonic setting (e.g., Grimes et al., 2015), the oxidation state of magma (e.g., Trail et al., 2012), or the growth temperature using the Ti-in-zircon geothermometer (e.g., Aubrecht et al., 2017), collectively helping source-to-sink correlations. While the use of zircon as a provenance tool is generally supported by a vast amount of published data for comparison with potential crystalline source rocks, as well as detrital grains within intermediate age sediment storage, single-mineral provenance studies face a clear mineral-specific bias (e.g., Chew et al., 2020). Interpretations based on zircon can be biased towards overrepresentation of felsic to intermediate igneous rocks (e.g., Malkowski et al., 2019) and lithologies with high zircon abundance (fertility) (e.g., Moecher & Samson, 2006). Furthermore, the slow diffusion rate of Pb in zircon with a closure temperature of ca. 900°C restricts age resetting during most geological processes (Cherniak & Watson, 2001). This, and sparce zircon growth during low and medium grade metamorphic conditions (Kohn et al., 2015) renders the U–Pb zircon system relatively insensitive to most low-medium temperature processes. Therefore, detrital zircon poorly represents magma-poor orogens (e.g., O'Sullivan et al., 2016), potentially missing entire orogenic cycles within any catchment area (Krippner & Bahlburg, 2013).

The integrated analysis of additional mineral phases (e.g., rutile, apatite and monazite) that occur in a compositional range of source rocks can provide more accurate source-to-sink interpretations compared to those based on single-mineral analysis (e.g., Gillespie et al., 2018; Moecher et al., 2019; Rösel et al., 2014). Specifically, mineral pairs such as zircon-rutile that (i) record distinct geological processes and (ii) show similar hydrodynamical behaviour

(i.e., no differential fractionation) are favourable combinations (von Eynatten & Dunkl, 2012). Rutile, in comparison to zircon, is primarily sourced from metamorphic rocks (Force, 1980), and U–Pb analysis of rutile documents middle to lower crustal processes (e.g., Smye et al., 2018) due to the lower retentivity of Pb in rutile with a closure temperature of ca. 600°C (Cherniak, 2000). Such discrepancies of genesis and Pb retentivity between zircon and rutile render this combination effective to capture a wide range of geological processes taking place at different temperatures, ultimately resulting in more complete provenance information (see examples of coupled zircon-rutile applications in Bracciali, 2019). Additionally, trace elements in rutile act as excellent tracers of source rock protolith compositions (i.e., mafic versus pelitic; e.g., Triebold et al., 2012) and allows for estimation of growth temperatures using the Zr-in-rutile geothermometer (Tomkins et al., 2007).

A different approach to help define basement signatures could be through characterization of modern catchments within the study area (e.g., Malusà et al., 2016). Such an approach may provide important information not accessible in the currently exposed crystalline basement and hence provide a more distinctive source fingerprint. Moreover, erosional sampling of the crust in an area may provide a more representative sample of the basement age structure than direct dating of individual crystalline rocks (e.g., Pepper et al., 2016).

This work describes a multi-proxy approach analysing detrital zircon (U–Pb, Lu–Hf and trace elements) and detrital rutile minerals (U–Pb and trace elements) of the Lower Cretaceous Broome Sandstone and modern sedimentary systems in its proximity (Figure 2a). The work focuses on (i) establishing the provenance of detrital zircon and rutile of the Broome Sandstone, (ii) reconstructing the sediment routing system and contextualizing these results within the broader framework of previously published late Mesozoic sediment routing systems in Australia, and (iii) elucidating the controls and associated implications of post-Gondwanan changes in the sediment drainage patterns in Australia.

2 | GEOLOGICAL FRAMEWORK

2.1 | The Canning Basin

The NW-SE trending Canning Basin in NW Australia comprises a ca. 430,000 km^2 area of Ordovician to Cretaceous

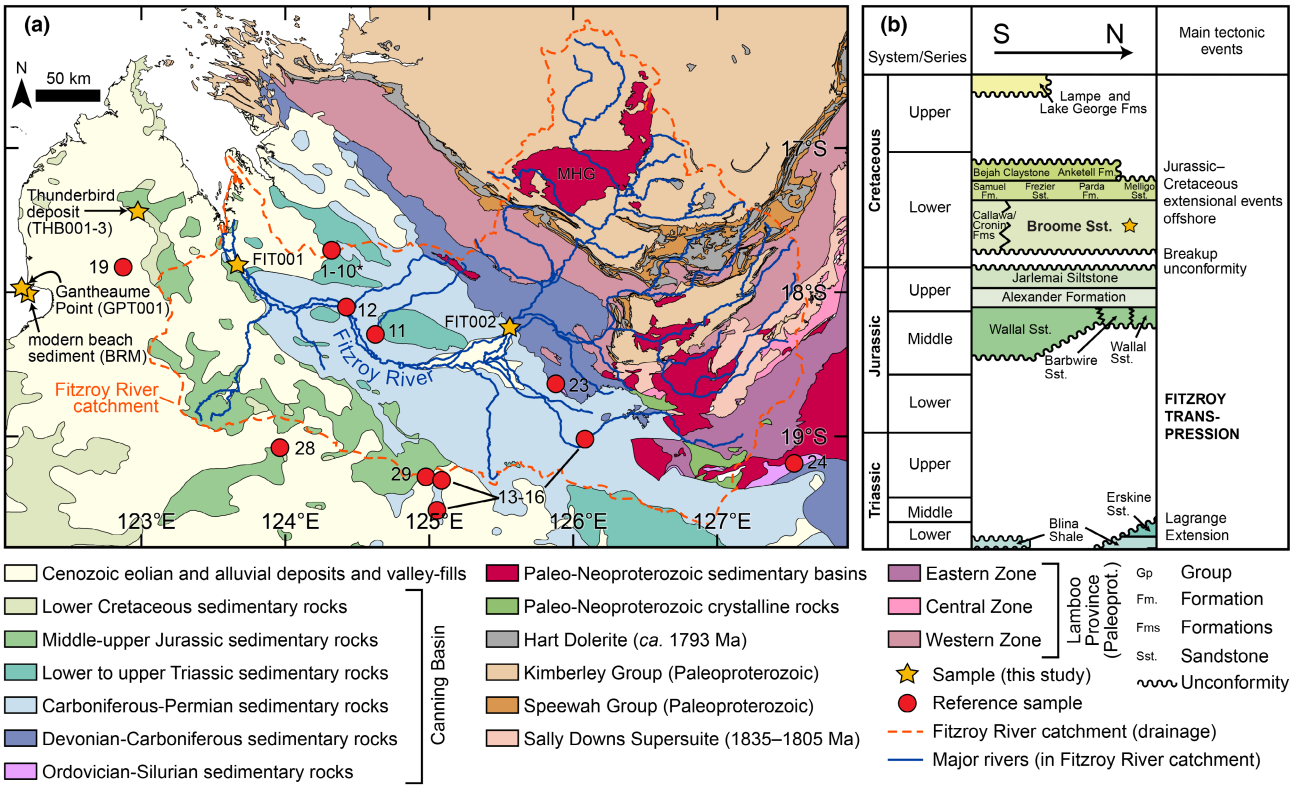

FIGURE 2 (a) Geological map of the study area with sample locations (yellow stars) and drainage area of the Fitzroy River. Red dots show reference sample locations (Figure 9 and Table S3). MHG, Mount House Group (Cryogenian-Ediacaran). (b) Mesozoic stratigraphy and the main tectonic events of the Canning Basin (modified after Mory & Hocking, 2011). Arrow indicates spatial occurrence of sedimentary units within the basin; S, South; N, North.

sedimentary rocks (Figure 1c) with a maximum sediment thickness of ca. 15 km (Forman & Wales, 1981). The evolution of the Canning Basin can be subdivided into at least seven major tectonic phases (Hashimoto et al., 2018): (i) Early Ordovician–Silurian extension and subsidence, (ii) middle Silurian–Early Devonian uplift and erosion, (iii) Devonian–early Carboniferous extension and subsidence, (iv) Middle Carboniferous transpression, uplift and erosion, (v) Late Carboniferous–Triassic extension and subsidence, (vi) Early Jurassic transpression, uplift and erosion and (vii) Middle Jurassic–Cenozoic breakup and passive margin.

The early Mesozoic sedimentary record of the Canning Basin is limited to transgressive fluvio-deltaic sandstones and shallow marine mud- and sandstones (Erskine Sandstone and Blina Shale, respectively), deposited during the Early Triassic (Figure 2b). Early Mesozoic sedimentation ceased with the onset of the Fitzroy Transpressional Movement initiating widespread deformation and erosion, especially affecting the northern parts of the basin (Parra Garcia et al., 2014). In response to subsidence, sedimentation resumed during the Middle Jurassic and resulted in deposition of deltaic, fluvial and aeolian sedimentary successions of the Wallal and Barbwire sandstones (Hashimoto et al., 2018). These sediments are overlain by the transgressive shallow marine to paralic Alexander Formation and Jarlemai Siltstone (Figure 2b), deposition of which was followed by marine regression and minimal additional sedimentation until the Early Cretaceous (Forman & Wales, 1981). After the separation of Australia and Greater India, the Canning Basin became a passive margin (Hashimoto et al., 2018). During the Valanginian–Barremian transgression, the shallow marine to paralic rocks of the Broome Sandstone, interpreted in the context of a northwest to westward-prograding fluvio-deltaic system (Forman & Wales, 1981; Hashimoto et al., 2018; Salisbury et al., 2016; Smith et al., 2013), were deposited. The Broome Sandstone records the occurrence of dinosaur ichnofauna (e.g., Salisbury et al., 2016), and hosts heavy mineral sand deposits of economic relevance (Boyd & Teakle, 2016).

2.2 | Potential areas of sediment generation

The onshore Canning Basin is framed by several crystalline and sedimentary packages of different age and formation history. Crystalline basement rocks, that may represent areas of primary sediment generation (ultimate crystalline sources) bordering the Canning Basin, can be broadly divided into Archean, Paleo–Mesoproterozoic, and/or Neoproterozoic–early Phanerozoic lithologies (Figure 1b).

2.2.1 | Archean sources

The principal possible sources for Archean detritus supply to the Canning Basin are the Pilbara and Yilgarn cratons. The crystalline part of the Pilbara Craton consists of granite-greenstone terranes, largely formed during the Paleo–Mesoarchean at ca. 3530–3070 Ma (e.g., Champion & Smithies, 2007), and post-orogenic granitoids formed at ca. 2890–2830 Ma (Hickman & van Kranendonk, 2012). The Yilgarn Craton records major crustal growth at ca. 2730–2620 Ma (Cassidy et al., 2006). Further Archean sediment sources, albeit volumetrically insignificant compared to the Pilbara and Yilgarn cratons, can be found in the Granites-Tanami region, which generally comprises rocks of Paleoproterozoic age (e.g., Bagas et al., 2009), but contains ca. 2514 Ma orthogneisses (Smith, 2001).

2.2.2 | Paleo–Mesoproterozoic sources

Several sources of Paleo–Mesoproterozoic material are distributed along the fringes of the Canning Basin. In the northeast, the Kimberley region (Figure 1b) records the ca. 1870–1850 Ma Hooper Orogeny, the ca. 1835–1805 Ma Halls Creek Orogeny, and ca. 1865–1850 Ma felsic magmatism of the Paperbark Supersuite, all part of the Lamboo Province (Hollis et al., 2014; Tyler et al., 2012). In the east, the Arunta region forms the southern part of the North Australian Craton and hosts the ca. 1860–1700 Ma Aileron and the ca. 1690–1600 Ma Warumpi provinces (Collins, 1995; Hollis et al., 2013). Paleo–Mesoproterozoic basement lithologies around the western flank of Canning Basin are the Capricorn Orogen and the Rudall Province (Figure 1b). The Capricorn Orogen documents the collision of the Pilbara and Yilgarn cratons with tectonomagmatic events at ca. 2200 Ma, 2000–1960 Ma and 1830–1780 Ma (Cawood & Tyler, 2004). The Rudall Province, east of the Capricorn Orogen, documents zircon U–Pb age modes at ca. 1804–1762 Ma, 1589–1549 Ma, 1310–1286 Ma and 1185–1165 Ma (Gardiner et al., 2018; Kirkland, Johnson, et al., 2013; Payne et al., 2021). The Musgrave Province in central Australia, on the edge of the Canning Basin to the south, presents a Paleo– and Mesoproterozoic history characterized by the ca. 1345–1293 Ma Mount West Orogeny, the ca. 1220–1150 Ma Musgrave Orogeny, and the ca. 1090–1040 Ma Giles Event (Howard et al., 2015; Kirkland, Smithies, et al., 2013; Smithies et al., 2015). A more distal, but also plausible source, are igneous rocks of the Proterozoic Albany-Fraser Orogen located on the very southern end of the Canning Basin. Lithologies of the Albany-Fraser Orogen document major zircon age modes at 1710–1650 Ma,

1345–1260 Ma and 1215–1140 Ma (Kirkland et al., 2011; Spaggiari et al., 2015).

2.2.3 | Neoproterozoic–early Phanerozoic sources

The ca. 750–720 Ma Miles Orogeny (Rudall Province; Bagas, 2004), the ca. 600–530 Ma Petermann Orogeny (Musgrave Province; Wade et al., 2006), the ca. 560 Ma Wunaamin Miliwundi Orogeny (Kimberley region; Tyler et al., 2012), and the ca. 550 Ma Paterson Orogeny (Rudall Province; Bagas, 2004) are all developed adjacent to the borders of the Canning Basin (Figure 1b). Based on the broad temporal overlap of these orogenic events, as well as geophysical indications of a continuity between these spatially separated geological units, a coherent transcontinental orogenic system (Paterson-Petermann orogenic belt) has been suggested (e.g., Martin et al., 2017). The youngest major tectonometamorphic event of the study area is the polyphased Alice Springs Orogeny in central Australia at ca. 450–300 Ma (Buick et al., 2008).

2.2.4 | Sources of recycled detritus

Numerous sedimentary basins frame and underlie the Canning Basin and can be considered potential sources of recycled detritus (intermediate sources). Proximal extra-basinal sources of recycled sedimentary detritus are the Kimberley and Speewah groups that account for large parts of the Kimberley region (Figure 2a) and show detrital zircon age spectra dominated by age modes at ca. 2525–2480 Ma and ca. 1880–1850 Ma (Hollis et al., 2014). Sediments from central Australia, such as those corresponding to the Amadeus Basin and Officer Basin, are additional probable sources of recycled sediments. Both basins' detrital zircon age distributions are interpreted to reflect substantial sediment supply from the Musgrave Province (detrital zircon ages at ca. 1200–1000 Ma) and the Arunta region (ca. 1860–1700 Ma and 1690–1600 Ma) (Haines et al., 2013, 2016; Maidment et al., 2007). The Palaeozoic of the Officer Basin also includes a significant portion of ca. 700–500 Ma ages, potentially sourced from Antarctica (Haines et al., 2013; Morón et al., 2019). Intrabasinal recycling of Canning Basin sediments, perhaps through erosion during fluvial processes, is an additional feasible source of recycled detritus for successively younger units. Although different sedimentary successions throughout the Canning Basin show distinct detrital zircon spectra, most analysed Canning Basin lithostratigraphic units are dominated by three major age modes at ca. 1800–1500 Ma, 1250–1000 Ma and 700–500 Ma (Haines et al., 2013; Morón et al., 2019).

2.3 | Gondwanan sediment routing of the Canning Basin

The oldest deposits of the Canning Basin, principally formed during the Ordovician, show distinct detrital zircon age signatures in northern and southern parts of the basin. Northern sedimentary rocks of the Canning Basin (locations 23 and 24 in Figure 1b) show detrital age compositions similar to local sources suggesting proximal sediment supply (Haines et al., 2013). In contrast, detrital zircon age spectra of Ordovician sediments in the southeast Canning Basin (locations 25–28 in Figure 1b) are similar to the western Officer Basin age distributions, which contain ca. 700–500 Ma detrital zircon grains that have been linked to source rocks in Antarctica (e.g., Cawood & Nemchin, 2000; Haines et al., 2013; Veevers, 2018). These observations are interpreted as sediment routing of ultimately Antarctica-derived detritus into the southeast of the Canning Basin via the Officer Basin (Haines et al., 2013). Similar detrital zircon age patterns are seen for Silurian to Permian sedimentary successions (locations 17–21 in Figure 1b) of the Canning Basin (Haines et al., 2013). Glaciogenic sediments of the early Permian Grant Group of the Canning Basin (locations 13–16 in Figure 1b) show detrital zircon fingerprints broadly similar to those of older Canning Basin sediments, but tend towards a dominance of central Australian sources, such as Arunta region, Musgrave Province and Alice Springs Orogen (Martin et al., 2019). Likewise, detrital zircon ages from the Triassic Erskine Sandstone (locations 1–10 in Figure 1b) reveal qualitatively similar source constraints compared to the overall Canning Basin trend but show distinct local age signals from the proximal Wunaamin Miliwundi Orogen (Thomas, 2012). However, based on the high similarity of detrital zircon age and Lu–Hf data within Palaeozoic to early Mesozoic (Triassic) sedimentary successions of the Canning Basin and proximal sedimentary units (e.g., Carnarvon Basin, Lhasa Terrane), as well as channel-belt thickness scaling relationships, a long-lived transcontinental sediment routing system has been suggested to have discharged onto the Northwest Shelf through the Canning Basin (see figure 1 in Morón et al., 2019). This large-scale sediment routing system is interpreted to include a south-to-north system sourcing sediments from Antarctica and a system supplying detritus from central Australia (Morón et al., 2019). A significant degree of intermediate storage and recycling

of Antarctica-derived material has been proposed on the basis of characteristic detritus in southwestern Australia (Kirkland et al., 2020).

2.4 | The catchment of the Fitzroy River

The catchment of the sampled Fitzroy River measures ca. 94,000 km^2 and represents the largest drainage system in present-day NW Australia (Figure 2a). The catchment of the river is principally considered non-perennial (Crossman & Li, 2015), with widespread over bank flood events in the catchment during the wet season and summer tropical cyclones (Wohl et al., 1994). The drainage area of the Fitzroy River can be separated into two components based on underlying crust. The lithologies of the upstream SW draining river system are mostly Paleoproterozoic in age and are part of the Kimberley region (Figure 2a). The lower part of the Fitzroy River heads NW and flows through sedimentary rocks of the Canning Basin, as well as younger, often poorly consolidated sediments, which comprise Cenozoic aeolian and alluvial deposits and/or valley-fills (Figure 2a).

3 | METHODS AND MATERIALS

This work studied four samples of the Cretaceous Broome Sandstone, three samples from modern sediments (Figure 2a), and analysed a total of 1500 detrital minerals. Three unconsolidated samples (THB001-003) are from a littoral heavy mineral placer deposit (Thunderbird) hosted within the clastic strata of the Broome Sandstone (Boyd & Teakle, 2016). Another sample of the Broome Sandstone has been collected from an outcrop at Gantheaume Point (GPT001). Modern samples of fluvial (Fitzroy River; FIT001 [downstream] and FIT002 [upstream]; Figure 2a) and littoral (Broome; BRM) sands have been selected to capture the detrital fingerprint of the modern catchment. Specifically, the modern detrital signature may help to resolve source signatures of the proximal Kimberley region and other sources of near-contemporaneous formation (e.g., the distal Arunta region). Minerals of the sandstone sample GPT001 have been liberated using high voltage electrical fragmentation (SelFrag Lab, Switzerland). Subsequent steps of mineral separation were identical for all disaggregated sediment samples and involved the use of a Jasper Canyon Research zircon shaking table (Dumitru, 2016), heavy liquid separation (density of 2.85 g/cm^3), and a single-step magnetic separation using a Frantz isodynamic magnetic separator at 1 A using a side slope and slope of 10° and 15°, respectively. Representative splits of the heavy mineral separates for most samples were bulk-mounted, with grains randomly affixed on double-sided tape and embedded in epoxy resin. Zircon grains of sample BRM were hand-picked. Also, one rock chip (whole rock, ca. 1 cm diameter) of the Broome Sandstone outcrop sample (GPT001) was embedded in an epoxy mount. Subsequently, mounts were polished to expose grain interiors. Mineralogical identification and mapping were performed using energy-dispersive X-ray spectrometry (EDX) and backscattered electron imaging on the TESCAN Integrated Mineral Analyser (TIMA).

The multi-proxy approach focusses on analyses of zircon and rutile minerals, which were analysed by laser ablation inductively coupled plasma mass spectrometer at the GeoHistory Facility in the John de Laeter Centre, Curtin University (Perth, Australia). Analyses of detrital zircon include measurement of their U–Pb and Lu-Hf isotopic composition, as well as quantification of their trace element composition. Zircon spot analyses have been guided by cathodoluminescence imaging using a TESCAN Clara FE-SEM. If different growth zones (i.e., core-rim zonation) were observed, rims of zircon grains sufficiently large to host a laser spot were targeted for analysis. Detrital rutile were analysed for their U–Pb and trace element compositions. Rutile analyses were performed for TiO_2 grains (as identified by TIMA) that showed homogenous backscattered electron response, absence of superficial inclusions and no obvious signs of alteration. U–Pb ages were calculated using IsoplotR (Vermeesch, 2018). Concordia ages (Ludwig, 1998) are used to avoid changing between different ratios for age calculation, to make optimum use of both U/Pb and Pb/Pb ratios. The use of single analysis Concordia ages carries substantial advantages for the interpretation of detrital age data as shown by empirical and model-based demonstrations (Vermeesch, 2021; Zimmermann et al., 2018). All ages are quoted at 2σ absolute uncertainty. ^{204}Pb was used as a semi-quantitative screening tool for common Pb and was monitored during the data reduction. For concordant analyses, common Pb contents were found to be below detection limits and thus, zircon age data are not corrected for common Pb. Calculation of εHf values use the Chondritic Uniform Reservoir composition of Bouvier et al. (2008) and the ^{176}Lu decay constant of Söderlund et al. (2004). Post-analysis identification of the TiO_2 phases (i.e., rutile, brookite and anatase) was accomplished by applying the trace element-based discrimination of Triebold et al. (2011). Rutile age data are corrected for common Pb using a ^{208}Pb-correction (Zack et al., 2011) for rutile grains displaying Th/U < 0.1. Rutile analyses exceeding this threshold, are not considered for further investigation as high Th content are unusual in primary metamorphic rutile (Zack et al., 2011), and possibly induced by secondary overprinting and/or inclusions. Zircon and rutile growth

temperatures have been calculated (assuming activities at unity) using the Ti-in-zircon and Zr-in-rutile (at 10 kbar) geothermometers of Watson et al. (2006) and Tomkins et al. (2007), respectively. Sample site locations and analytical methods employed for each sample are summarized in Table 1. Full documentation of analytical procedures is provided in Supporting Information S1 and the results of reference materials are listed in Table S2 in Supporting Information S2.

4 | RESULTS

4.1 | Mineralogical composition

The mineralogy of the Broome Sandstone (whole rock), based on EDX analysis of a rock chip, is dominated by Quartz (ca. 81%). Clay minerals (likely Kaolinite) and feldspar (mostly K-feldspar) account for ca. 7% and 6%, respectively. Ilmenite, TiO_2 polymorphs and zircon are the dominant accessory minerals as documented in the heavy mineral composition (Table 2). Other, minor accessory phases are tourmaline, monazite and Al_2SiO_5 polymorphs. The major phases of the heavy mineral concentrate of the upstream Fitzroy River sediment are ilmenite (ca. 48%), haematite/magnetite (ca. 13%) and unclassified, potentially altered grains (ca. 11%). The upstream Fitzroy River sample contains only modest occurrences of ultrastable minerals (e.g., TiO_2 polymorphs, zircon and tourmaline) compared to the downstream sample. The latter is also dominated by ilmenite (ca. 40%) but reveals ca. 15% TiO_2 polymorphs and 11% zircon among the heavy minerals. The complete mineralogical compositions, based on EDX, are provided in Table 2.

4.2 | Detrital zircon

4.2.1 | U–Pb geochronology

Most samples reveal polymodal age spectra (Figure 3). There is a total of 443 concordant ages out of 868 measurements. In the following, concordant ages are interpreted as magmatic emplacement ages of source rocks or ages of metamorphism in source areas. All four samples of the Lower Cretaceous Broome Sandstone show similar detrital zircon U–Pb age distributions (Figure 3). U–Pb zircon ages of the Broome Sandstone range from early Permian (youngest grain 298 ± 3 Ma) to Paleoarchean (oldest grain ca. 3362 ± 18 Ma). Major age modes, approximated

TABLE 1 Sample sites and employed methodology

Sample ID	Sample	Age	Lat	Long	Method(s)
Broome Sandstone					
THB001	Thunderbird deposit, sand (3.5–8.6 m depth)	Valanginian–Barremian[a]	17°25′41.52″S	122°57′47.52″E	Zircon (U–Pb, Lu–Hf), Rutile (U–Pb, Trace elements)
THB002	Thunderbird deposit, sand (8.6–11.4 m depth)	Valanginian–Barremian[a]	17°25′41.52″S	122°57′47.52″E	Zircon (U–Pb, Lu–Hf), Rutile (U–Pb, Trace elements)
THB003	Thunderbird deposit, sand (8.2–11.1 m depth)	Valanginian–Barremian[a]	17°26′2.40″S	122°57′50.04″E	Zircon (U–Pb, Lu–Hf), Rutile (U–Pb, Trace elements)
GPT001	Gantheaume Point, sandstone	Valanginian–Barremian[a]	17°58′25.96″S	122°10′33.53″E	Zircon (U–Pb, Trace elements), Rutile (U–Pb, Trace elements)
Riverine					
FIT001	Fitzroy River sand, downstream	Modern	17°44′2.13″S	123°38′53.56″E	Zircon (U–Pb, Trace elements), Rutile (U–Pb, Trace elements)
FIT002	Fitzroy River sand, upstream	Modern	18°11′20.82″S	125°35′8.02″E	Zircon (U–Pb, Trace elements), Rutile (U–Pb, Trace elements)
Coastal					
BRM	Broome beach sand	Modern	18°00′23.5″S	122°12′38.8″E	Zircon (U–Pb)

[a]Broome Sandstone age of deposition (ca. 140–127 Ma) based on palynological constraints (Smith et al., 2013).

TABLE 2 Mineralogical composition obtained from whole rock (WR) and/or heavy mineral (HM) analysis utilizing energy-dispersive X-ray spectrometry using the TESCAN Integrated Mineral Analyser (TIMA)

Mineral phase	GPT001 (WR)	GPT001 (HM)	FIT001 (HM)	FIT002 (HM)
Quartz	80.8	2.8	2.5	1.4
Clay (Kaolinite?)	6.6	0.2	0.0	0.0
K-feldspar	5.0	0.1	0.1	0.2
Al_2SiO_5-Polymorph	2.5	0.6	0.6	0.3
Plagioclase	0.5	2.3	7.6	4.6
Ilmenite	0.4	66.9	40.0	47.8
Garnet	0.2	0.1	1.8	3.0
TiO_2-Polymorph	0.2	8.7	14.5	2.2
Tourmaline	0.2	1.9	2.2	1.0
Biotite	0.1	0.0	2.9	4.2
Zircon	0.1	10.9	10.5	1.3
Haematite/Magnetite	0.0	0.1	3.5	12.8
Monazite	0.0	1.1	0.4	0.1
Amphibole	0.0	0.0	2.7	3.7
Pyroxene	0.0	0.0	1.4	3.5
Titanite	0.0	0.0	0.8	1.0
Unclassified/Altered	1.5	2.4	6.3	10.5
Other phases	2.1	2.0	2.2	2.3
Total	100	100	100	100

from kernel density estimates, present in the Broome Sandstone are at ca. 2760–2590 Ma, 1930–1700 Ma, 1690–1430 Ma, 1350–1000 Ma, 710–510 Ma and 450–300 Ma. The main age mode of Broome Sandstone samples is at ca. 1350–1000 Ma (ca. 41%) with a maximum at ca. 1180 Ma. The prevalent age modes and the age distribution of the Broome Sandstone detrital zircon are consistent with an unpublished U–Pb zircon dataset of the outcropping Broome Sandstone near Broome (Bodorkos, 2011; Sample No 2115398), which is available through Geoscience Australia (ga.gov.au/geochron-sapub-web/geochronology/shrimp/search.htm). The modern samples analysed in this study have distinct U–Pb age distributions. The beach sample (BRM) is dominated by U–Pb ages of ca. 1150 Ma. The Fitzroy River samples differ significantly; while the downstream sample age distribution is strongly polymodal and qualitatively comparable to those of the Broome Sandstone, the upstream sample shows a dominance of the ca. 1930–1700 Ma age mode (Figure 3). Concordia diagrams of all zircon analyses are shown in Figure S1 (in Supporting Information S1), and full results are provided in Table S1 (in Supporting Information S2).

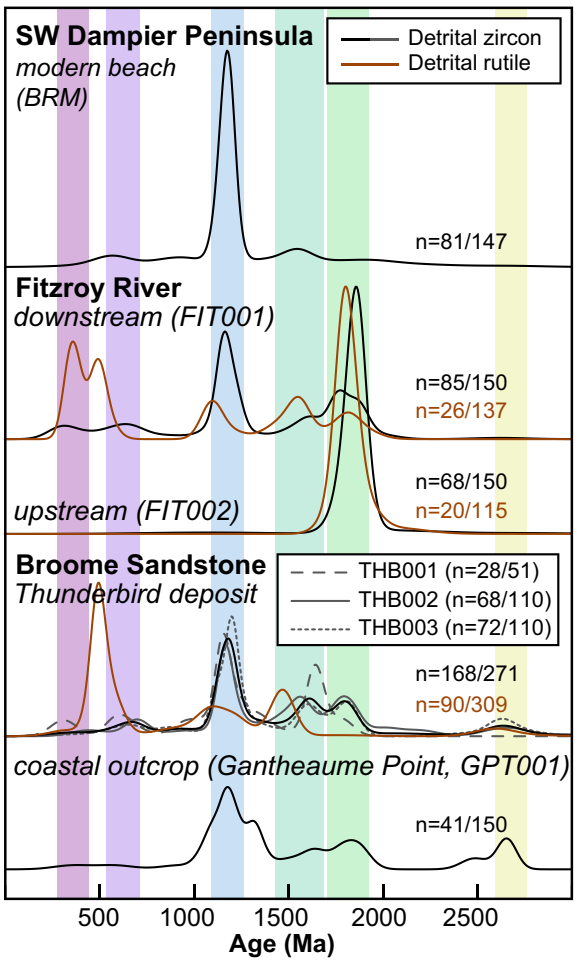

FIGURE 3 Normalized kernel density estimates of U–Pb ages of concordant detrital zircon (black and grey lines) and concordant detrital rutile (brown lines). Vertical colour bars show main age modes of detrital zircon as discussed and used in Figure 9 (the visualization of main age modes of detrital rutile is found in Figure S1). *N*, Number of analyses (concordant/total; for rutile total numbers refers to TiO_2 grains classified [based on trace element composition] as rutile).

4.2.2 | Lu–Hf isotope geochemistry

About 76% of the zircon Hf isotope data, only measured for the Broome Sandstone samples (Table 1), range between moderately radiogenic to moderately unradiogenic $\varepsilon Hf_{(t)}$ values (5 to −5, Figure 4). Generally, detrital zircon older than ca. 1500 Ma tend to show evolved Hf signatures (− $\varepsilon Hf_{(t)}$), while younger grains have juvenile Hf isotopic compositions (+ $\varepsilon Hf_{(t)}$). The main data cluster at around ca. 1150 Ma shows $\varepsilon Hf_{(t)}$ values between ca. 5 and −6 with a median value of ca. 1.8, which is interpreted as a juvenile source of chondritic-like composition. There are several smaller, mostly sub-chondritic, clusters between ca. 1900 and 1500 Ma. Full results are provided in Table S1.

4.2.3 | Trace elements

The detrital zircon of the Broome Sandstone show trace element compositions that resemble those of the modern Fitzroy River upstream and downstream sediment samples (Figures S4a,c and S5). The scatterplots of trace element concentrations and ratios sensitive to different tectonic settings (Figure S4a,c) reveal a broad cluster with no distinct sub-clusters. Many detrital zircon trace element compositions are consistent with zircons of granitoids formed within continental crust or magmatic arc settings (Figure S4). Zircon grains with ages around the prevalent ca. 1150 Ma age mode plot closer to the 'oceanic crust zircon' and 'mantle-zircon array' discrimination fields of Grimes et al. (2007) and Grimes et al. (2015), respectively, than other age modes (Figure S4b,d). Ti-in-zircon temperatures show a broad scatter for most time intervals (Figure 5a), although younger ages (710 to 300 Ma) appear to show lower growth temperatures compared to older zircon analyses. Other frequently used trace element ratios, such as Th/U, U/Yb, Lu/Nd, Zr/Hf, Eu/Eu* (Eu anomaly) and Ce/Ce* (Ce anomaly) show no distinct trends with no sub-clusters to divide individual age modes (Figure S5). Full results are provided in Table S1.

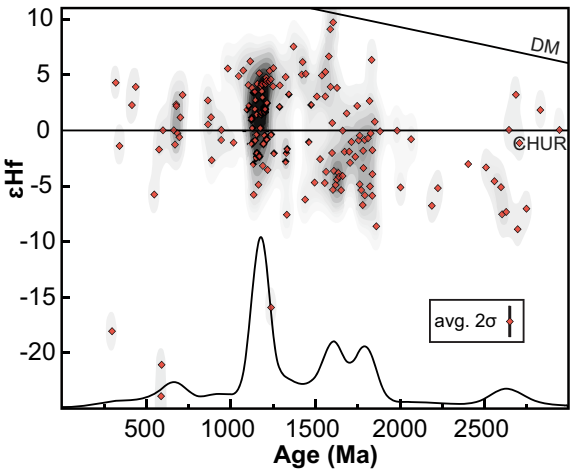

FIGURE 4 Hf isotope compositions of concordant detrital zircon from the Broome Sandstone (samples THB001, THB002 and THB003). Red diamonds represent individual analyses. These have been used to render the grey bivariate kernel density estimate that is masked at its 95% peak density contour. Dark and light grey reflect high and low density, respectively. Black curved line is a univariate kernel density estimate of U–Pb ages of detrital zircon of the Broome Sandstone (Figure 3). Depleted mantle (DM) and chondritic uniform reservoir (CHUR) values after Griffin et al. (2000) and Bouvier et al. (2008), respectively. Visualized using HafniumPlotter (Sundell et al., 2019).

4.3 | Detrital rutile

4.3.1 | U–Pb geochronology

Approximately 80% of 705 measurements of TiO_2 mineral phases were classified as rutile. About 38% of rutile analysis display Th/U < 0.1 and in total 135 concordant rutile ages (of 561 rutile analyses) have been obtained. Rutile ages within the Broome Sandstone range from 2757 ± 71 Ma to 326 ± 21 Ma. The Broome Sandstone rutile age spectrum is polymodal with major age modes, based on kernel density estimates, at ca. 2760–2540 Ma, 1930–1690 Ma, 1580–1400 Ma, 1270–1100 Ma, 610–440 Ma and 400–320 Ma (Figures 3 and S2). The dominant age mode (ca. 43% of

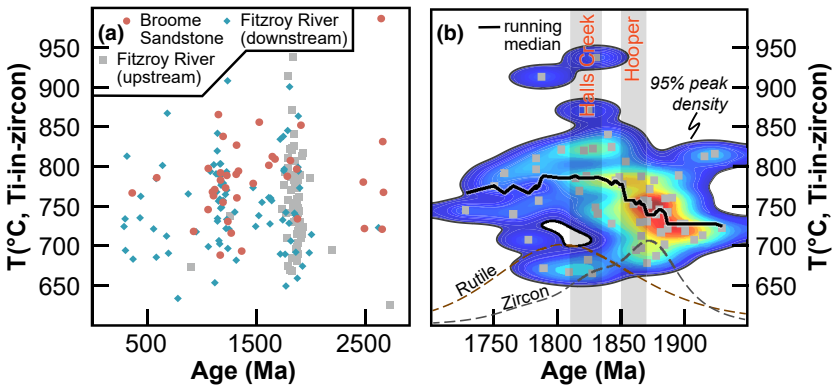

FIGURE 5 (a) Age-constrained results of Ti-in-zircon thermometry of concordant detrital zircon from the Broome Sandstone (GPT001) and Fitzroy River downstream (FIT001) and upstream (FIT002) sediments. Temperature estimates based on the geothermometer of Watson et al. (2006). (b) Ti-in-zircon temperature against age of concordant zircon grains in sample FIT002 (Fitzroy River, upstream) within the age range 1950–1700 Ma. Colours show intensity of bivariate kernel density estimate; red and blue reflect high and low density, respectively. Grey bars show timing of Halls Creek (1832–1805 Ma) and Hooper Orogeny (1870–1850 Ma). Running median is based on 15 datapoints. Grey and brown dashed line are kernel density estimates of U–Pb ages of detrital zircon and detrital rutile within sample FIT002, respectively (Figure 3).

data) ranges from ca. 610 to 440 Ma and shows a maximum at ca. 500 Ma, which is interpreted as the timing for the late stage of the most recent large-scale metamorphic event affecting the source area of the Broome Sandstone. The detrital rutile age distributions of the Fitzroy River samples are distinct (Figure 3). While the upstream sample (FIT002) shows a unimodal distribution with a maximum at ca. 1810 Ma, the downstream (sample FIT001) detrital rutile age spectra is polymodal. The detrital rutile age distribution of the modern Fitzroy River downstream sample shares some major age modes with the Broome Sandstone age spectra but shows significantly higher proportions of the ca. 1930–1690 Ma (15%) and 400–320 Ma (23%) age modes (compared to 1% and 3%, respectively). Concordia diagrams of all rutile analyses are shown in Figure S3, and full results are provided in Table S1.

4.3.2 | Trace elements

On the basis of the Cr and Nb trace element composition (Triebold et al., 2012), the majority of analysed detrital rutile grains from the Broome Sandstone are of apparent pelitic origin (derived from a metamorphic source that had a pelitic protolith; Figure 6a). There are only a few rutile grains in the Broome Sandstone detritus that were derived from metamafic lithologies suggesting dominantly metapelitic source rocks for the detrital rutile cargo. The Fitzroy River upstream sample contains the highest proportion of mafic detrital rutile minerals, followed by the Broome Sandstone and the Fitzroy River downstream sample (Figure 6b). No apparent correlation between age and Cr and Nb concentrations is noted (Figure 6b). Zr-in-rutile temperatures show no distinct sub-clusters among most age groups, but show a high spread of temperatures within the main ca. 610–440 Ma age mode that seems to include a sub-cluster of rutile grains formed under high temperatures (ca. granulite) conditions (Figure 6c). No correlation between source rock protolith (mafic versus pelitic) and Zr-in-rutile temperatures were observed (Figure 6d). Full results are provided in Table S1.

5 | DISCUSSION

5.1 | Ultimate (crystalline) sources of Broome Sandstone sediments

The detrital age spectra and (isotope) geochemical proxies of the Broome Sandstone sediments show a diverse composition, suggesting multiple crystalline basement rocks as potential sources. The polyphase and complex evolution of possible source areas, where individual terranes contain several characteristic age modes partly overlapping with other potential source areas, may obfuscate interpretation of individual provenance proxies. Hence, confident identification of the source areas requires integration of the different proxies acquired and detailed contextualization with the regional geology. This section aims to discuss source-to-sink correlations of ultimate sources (i.e., original crystalline basement rocks) of the Broome Sandstone detritus. Importantly, such interpretations do not imply immediate sediment transfer between the inferred crystalline sources and the Broome Sandstone. Subsequent sections consider potential intermediate (sedimentary) sources for recycled detritus (Section 5.2).

A potential proximal source area, the Kimberley region, containing widespread sedimentary basins and suites of igneous and metamorphic rocks, appears to be only of subordinate relevance as a sediment source of the Broome Sandstone. Broome Sandstone detrital zircon U–Pb and Lu–Hf data show only marginal overlap with the compositions of the Kimberley and Speewah groups and the Halls Creek Orogen (Figure 7). However, given the widespread occurrence of Paleoproterozoic crystalline rocks around the Canning Basin, a more robust conclusion of local sediment supply can be derived from the integration with results from sands of the Fitzroy River. The upper drainage area includes parts of the Kimberley region (Figure 2a) and thus, the upstream sediments can be assumed indicative for a Kimberley source signal (at least for the present day). The distribution of the main mode of the upstream detrital zircon age spectrum (i.e., 1930–1700 Ma) is skewed towards younger ages (Figure 5b). Over-dispersion (mean square weighted deviation of ca. 25; Table S1) of the Paleoproterozoic age mode in the upstream sediments suggests the age distribution does not represent an individual source. On the basis of U–Pb geochronology and integration with trace elements (Ti-in-zircon, Figure 5b), the upstream sample's ca. 1930–1700 Ma age mode (91% of the full age spectra) is interpreted to comprise three populations with distinct provenance (Figure 8). The largest population at ca. 1900–1850 Ma and ca. 750°C is broadly consistent with the timing of the Hooper Orogeny (Figure 8) and is accordingly interpreted to reflect the early accretionary history of the Kimberley region (Tyler et al., 2012). Ages between ca. 1850 and 1810 Ma show significantly higher median temperatures (ca. 800°C), a higher spread of temperatures (Figure 5b), and are interpreted as Halls Creek Orogen detritus, consistent with the high-temperature formation history (e.g., Bodorkos et al., 1999). The source for the youngest detrital zircon grains (<1800 Ma) in the upstream Fitzroy River sediments is uncertain, as there is no known significant formation of felsic rocks in the region of this age (Tyler et al., 2012). While a Kimberley

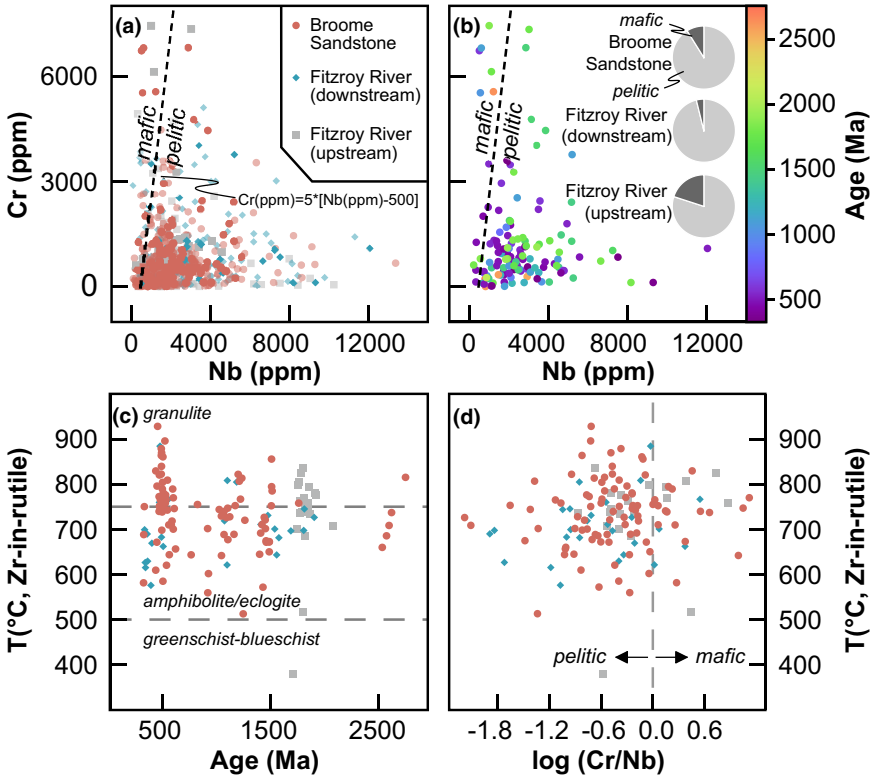

FIGURE 6 Results of trace elements analysis of detrital rutile from the Broome Sandstone (samples GPT001, THB001, THB002 and THB003) and Fitzroy River downstream (FIT001) and upstream (FIT002) sediments. (a) Cr versus Nb discrimination plot of rutile protolith after Triebold et al. (2012) using all detrital rutile trace element analyses. (b) Same plot using only concordant rutile analyses with colour-coded ages. Pie charts visualize proportion of concordant pelitic versus mafic rutile in the analysed samples showing a dominance of (meta)pelitic rutile protoliths. (c) Zr-in-rutile temperatures using the geothermometer of Tomkins et al. (2007) plotted against U–Pb age of concordant detrital rutile. (d) Zr-in-rutile temperatures plotted against protolith discrimination based on Cr and Nb trace element composition, positive log(Cr/Nb) values suggest an origin within metamafic rocks, while negative values suggest sourcing from metapelitic rocks (Meinhold et al., 2008).

source, perhaps the ca. 1793 Ma Hart Dolerite or felsic products (Ramsay et al., 2019) and recycling from the late Neoproterozoic Mount House Group or Palaeozoic rocks (Figure 2a), cannot be ruled out, exotic sources (e.g., Arunta region) are also possible. The ca. 1930–1700 Ma age mode of the Broome Sandstone only accounts for 15% of the entire spectrum and appears to be strongly diluted by ages not characteristic of the Kimberley region (Figure 8). This dilution effect suggests limited sourcing of Kimberley sediments. Furthermore, it was the Halls Creek Orogeny that affected the eastern Lamboo Province (Tyler et al., 2012) and the age distribution implies that sediment provenance was essentially restricted to this area. Additional evidence against significant Kimberley region contribution to the Broome Sandstone detritus is suggested by the absence of Paleoproterozoic detrital rutile ages, in contrast with the presence of these grains in both up- and downstream Fitzroy River samples (Figure 3). Consequently, Broome Sandstone sediments likely have a more distal derivation, perhaps associated with a large-scale routing system that swamps the proximal source signals.

Similarly, there is sparse evidence suggesting significant sediment derivation from the western flank of the Canning Basin. Paucity of detrital signatures corresponding to the Pilbara Craton (only a single detrital zircon >3000 Ma), situated proximal to Australia's NW shelf (Figure 1b), suggests sediment transfer via longshore drift is insignificant. Alternatively, the lack of Pilbara-derived detrital zircon may reflect the persistence of a now denuded sedimentary cover that limited bedrock exposure of the Archean craton (e.g., Morón et al., 2020), or minimal erosion of the Pilbara bedrock due to peneplanation (e.g., Sircombe & Freeman, 1999), perhaps in response to the preceding Permian glacial denudation.

Most recorded detrital Archean zircon grains show a signature corresponding to the Yilgarn Craton, located south of the Canning Basin. However, direct connection to the Yilgarn Craton is challenging to establish, as ultimate Yilgarn Craton-derived detritus is incorporated in

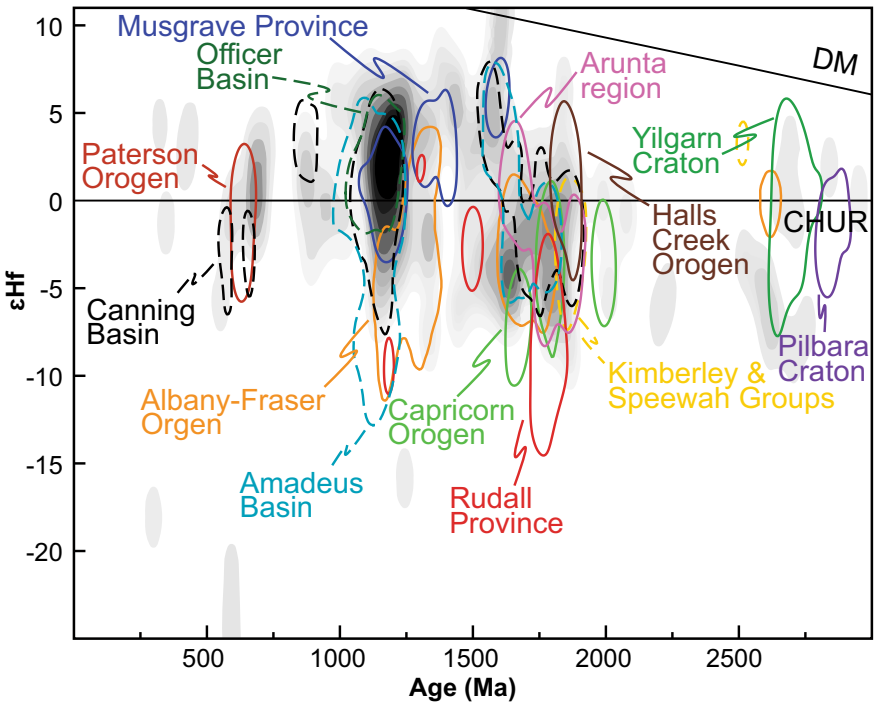

FIGURE 7 Hf isotope compositions of concordant detrital zircon from the Broome Sandstone (samples THB001, THB002 and THB003) compared to ultimate sources (crystalline rocks; solid lines) and intermediate sources (sedimentary rocks; dashes lines). Grey bivariate kernel density estimate, based on U–Pb age and Hf isotopic composition, shows the composition of the Broome Sandstone detrital zircon, and is masked at its 95% peak density contour (Figure 4). Dark and light grey reflect high and low density, respectively. Reference contours (coloured) correspond to 75% peak density with fixed kernel bandwidths (age = 25 Ma and εHf = 1.5). Kernel density estimates and contours were determined using HafniumPlotter (Sundell et al., 2019). DM and CHUR values after Griffin et al. (2000) and Bouvier et al. (2008), respectively. References for crystalline basement rocks: Albany-Fraser Orogen (n = 1515)—Kirkland et al. (2011), Spaggiari et al. (2015), dmp.wa.gov.au/Geochronology-1550.aspx; Paterson Orogen (n = 58)—Martin et al. (2017); Musgrave Province (n = 274)—Kirkland et al. (2013); Arunta region (n = 132)—Hollis et al. (2013); Capricorn Orogen (n = 569)—Johnson et al. (2017); Rudall Province (n = 480)—Kirkland et al. (2013), Gardiner et al. (2018), Tucker et al. (2018); Yilgarn Craton (n = 2055)—Mole et al. (2019) and references therein; Pilbara Craton (n = 443)—Nelson (2004), dmp.wa.gov.au/Geochronology-1550.aspx. References for sedimentary rocks: Canning Basin (n = 427)—Morón et al. (2019), Martin et al. (2019), dmp.wa.gov.au/Geochronology-1550.aspx; Amadeus Basin (n = 353)—Haines et al. (2016), dmp.wa.gov.au/Geochronology-1550.aspx; Officer Basin (n = 270)—dmp.wa.gov.au/Geochronology-1550.aspx; Kimberley region (n = 369)—Hollis et al. (2014).

several sedimentary basins and orogenic belts, for example the Capricorn Orogen (Johnson et al., 2017).

Sediment supply from the Capricorn Orogen may be implied by some overlap of Hf data of detrital zircon and Capricorn Orogen basement (Figure 7). However, this similarity represents a partial match with the Capricorn Orogen signature only, as parts of the indicative Hf contours correspond to low density of the Broome Sandstone Hf data. This, and the fact that most observed grains of Capricorn-like composition can be derived from other sources (e.g., Arunta or recycling of sedimentary basins) that show a higher similarity to areas of greater Hf data density (Figure 7), are interpreted to argue against dominant sediment supply of Capricorn Orogen sources.

Equally, the detrital Hf data do not indicate significant sediment supply from the Rudall Province, rooted on the Pilbara Craton (also on the western basin flank) due to only partial overlap in Hf-isotope space (Figure 7). A broad overlap of detrital zircon Hf compositions and Paterson Orogen granites (Martin et al., 2017) exists (Figure 7), but given the extensive presence of basically coeval ca. 700–500 Ma tectonometamorphic events (e.g., Petermann Orogeny, Figure 1b) and also limited number of grains of this age, the interpretive power for this component is limited. Ultimately, time-constrained zircon Hf data and absence of characteristic rutile ages suggest that rocks from the western hinterland of the Canning Basin appear not to have been a major contributor of detrital rutile and zircon.

In contrast to the low correlation to basement rocks along the western and northeastern borders of the Canning Basin, a central Australian ultimate crystalline basement provenance for the Broome Sandstone seems more feasible. The main age mode of detrital zircon at ca. 1350–1000 Ma with mostly juvenile Hf compositions

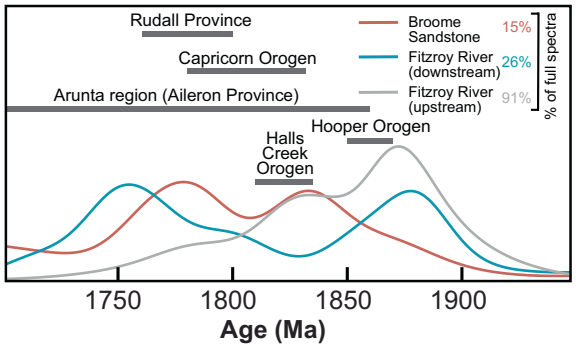

FIGURE 8 Normalized kernel density estimates of U–Pb ages of concordant detrital zircon in the age range 1950–1700 Ma that contains multiple potential source areas of broadly coeval age. Grey bars indicate characteristic age ranges of geological events of source areas. Percentages show the fraction of ages of the entire age spectra that are in the range of 1950–1700 Ma.

(Figure 4), is best explained by a dominant central Australian Musgrave Province (Kirkland, Smithies, et al., 2013) origin. Although the observed spread in the Hf data implies no unique Musgrave Province source for zircon ages of the 1350–1000 Ma age mode, this age mode comprises the highest median Ti-in-Zircon temperature (ca. 770°C) consistent with the high-temperature metamorphism and magmatism of the Musgrave Province (Howard et al., 2015). The alternative ultimate crystalline source, the largely coeval Proterozoic Albany-Fraser Orogen reveals more unradiogenic Hf signatures and significantly lower similarity to the Broome Sandstone detrital zircon Hf pattern than the Musgrave Province (Figure 7). Though the Albany-Fraser Orogen Hf envelopes cannot preclude this region as a more distal ultimate source for some of the detrital zircon, Albany-Fraser Orogen detritus is also present in some intermediate sources (dashed lines in Figure 7), meaning detritus may well be explained by sediment recycling within the Canning Basin catchment. Most of the ca. 1930–1700 Ma zircon grains show Hf signatures consistent with the Arunta region basement, also suggesting a central Australian source. Generally, rutile geochronology is consistent with central Australian sediment sources, given that the maxima of both the ca. 1580–1400 Ma and 1270–1000 Ma age modes occur shortly after zircon age maxima (Figure 3). This age pattern is a function of the lower closure temperature of rutile (compared to zircon) that is observed in cogenetic zircon-rutile pairs (e.g., Zhang, Mattinson, et al., 2014), and hence, indicative of a correlation to coherent sources. The dominant rutile age mode at ca. 610–440 Ma (peaking at ca. 496 Ma, Figure 3) showing the highest average growth temperatures (Figure 6c) is also consistent with a derivation from the central Australian Musgrave Province (Petermann Orogeny) that revealed rutile ages of ca. 498–472 Ma (Walsh et al., 2013). Furthermore, average growth temperature of recrystallized zircon rims of the Petermann Orogeny (Walsh et al., 2013) is 738 ± 18°C and comparable to the range of temperatures obtained for detrital zircons in the ca. 710–510 Ma age mode of this study (Figure 5a). Despite this, the vast extent of broadly coeval Neoproterozoic–early Phanerozoic sources, including the Canning Basin basement (Haines et al., 2018), renders robust source-to-sink correlation for the main rutile mode challenging. However, in tandem with detrital zircon fingerprint, a central Australian origin for the major rutile age mode appears the most likely explanation.

5.2 | Intermediate sources of recycled detritus

A central Australian sediment provenance does not necessarily imply direct (first-cycle) sourcing of crystalline basement lithologies and may be consistent with multi-cycle derivation (i.e., sediment recycling) of resistant detrital zircon and rutile. Significantly, detritus in sedimentary basins has often been subject to a myriad of sedimentary processes, for example physical and chemical weathering during transport, storage and diagenesis. These processes effectively remove labile phases and hence increase relative proportion of more resilient phases, such as zircon (e.g., Morton & Hallsworth, 1999). Thus, sediments may have similar or higher zircon cargo than crystalline basement rocks. Essentially, two endmember scenarios of sediment recycling that could result in the observed sediment characteristics exist: (i) intrabasinal sediment recycling (e.g., Auchter et al., 2020) of pre-Cretaceous Canning Basin strata and (ii) extra-basinal sediment recycling (e.g., Eriksson et al., 2004).

The likelihood of intrabasinal sediment recycling supplying detritus for the Broome Sandstone can be examined by comparison of new detrital zircon proxy data with published data of pre-Cretaceous Canning Basin sediments (Figure 9). Strata of the Canning Basin, particularly in the north, experienced uplift during the Jurassic that likely led to enhanced erosion of the basin sediments (Hashimoto et al., 2018). While substantial parallels of detrital zircon age modes between the Broome Sandstone and older sediments exist (Figure 9), some of these data originate from subsurface samples (Figure 1b) and, depending on stratigraphic position, are unlikely to reflect detrital signatures of possible intermediate sources available during the deposition of the Broome Sandstone (Figure 1c). Based on the stratigraphic record of the present-day Canning Basin, the exposed Carboniferous to early Mesozoic succession is a viable source for recycled sediments (Figure 1c). Multidimensional scaling (MDS; Figure 10a) of published

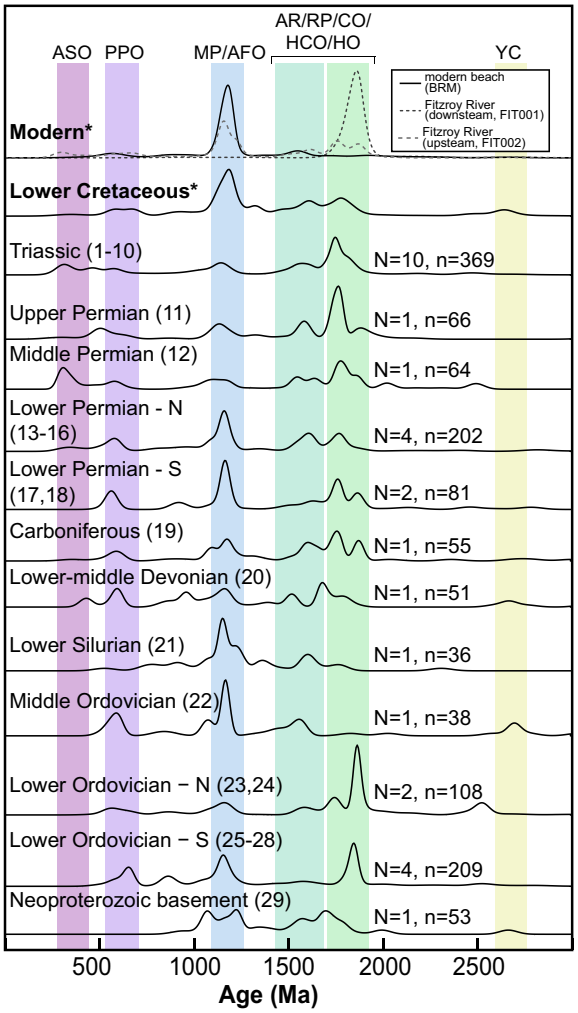

FIGURE 9 Normalized kernel density estimates of U–Pb ages of concordant detrital zircon of Canning Basin sediments and modern sediments. Vertical coloured bars show main age modes of detrital zircon (Figure 3) and possible ultimate crystalline sources for the age intervals. Numbers refer to locations in Figures 1 and 2; literature references are provided in Table S3 in Supporting Information S1. Lower Cretaceous includes samples GPT001, THB001, THB002 and THB003 of this study(*); *N*, Number of samples; *n*, Number of concordant analyses; ASO, Alice Springs Orogeny (e.g., Buick et al., 2008); PPO, Paterson-Petermann orogenic belt (e.g., Martin et al., 2017); MP, Musgrave Province (e.g., Kirkland, Smithies, et al., 2013); AFO, Albany-Fraser Orogen (e.g., Kirkland et al., 2011); AR, Arunta region (e.g., Hollis et al., 2013); RP, Rudall Province (e.g., Kirkland, Johnson, et al., 2013); CO, Capricorn Orogen (e.g., Cawood & Tyler, 2004); HCO, Halls Creek Orogen (e.g., Hollis et al., 2014); HO, Hooper Orogen (e.g., Hollis et al., 2014); YC, Yilgarn Craton (e.g., Mole et al., 2019).

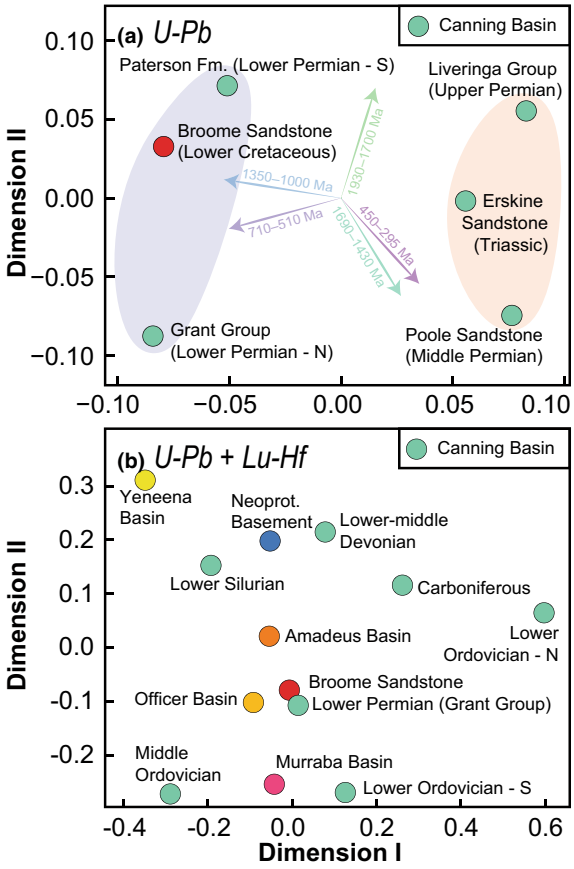

FIGURE 10 (a) Univariate multidimensional scaling of U–Pb ages of concordant detrital zircon of outcropping sediments of the Canning Basin (see literature references in Table S3) to compare potential intermediate (sedimentary) sources of recycled zircon grains and Broome Sandstone data to understand intrabasinal recycling in the Canning Basin. Schematic vectors show influence of age modes on position of individual age spectra. (b) Bivariate multidimensional scaling of integrated U–Pb and Lu–Hf isotopic information of concordant detrital zircon from Canning Basin sediments and surrounding sedimentary basins to help reveal recycling relationships. References are provided in the caption of Figure 4 and Table S3.

detrital zircon U–Pb age data reveals the similarity of the Broome Sandstone and lower Permian lithologies both in northern and southern areas of the Canning Basin. The MDS further indicates that similar age spectra are distinct from the middle–upper Permian units and the Triassic Erskine Sandstone, which are dominated by Paleoproterozoic-derived detrital zircon. However, MDS using univariate data, i.e., using U–Pb ages alone, where several potential sources are broadly coeval, is unlikely to provide a sophisticated sediment routing model. Bivariate statistical comparison integrating U–Pb and Lu–Hf data of detrital zircon may be a more robust tool (Sundell & Saylor, 2021) to understand the sediment routing system on a basin-wide scale. MDS using bivariate data of potential intermediate sources (Figure 10b) suggest, analogous to univariate MDS results, high similarity to the glaciogenic sediments of the lower Permian Grant Group located in the northern part of the basin. Greater distances (i.e., greater dissimilarity) from the Broome Sandstone are observed for pre-Permian Canning Basin sediments, and the Canning Basin basement (Figure 10b), suggesting

only moderate relevance for recycling of Canning Basin sediments (excluding Permian deposits) for source-to-sink correlation of the Broome Sandstone sediments. An additional perspective of intrabasinal recycling is provided by the detrital zircon and rutile age spectra of the downstream Fitzroy River sample. Those age spectra, vastly different to their upstream counterparts, reveal a significant mismatch to the corresponding basement geology of the catchment (Figure 2a). This mismatch is most likely related to a multi-cycle origin of the majority of the more resilient phases (e.g., zircon and rutile), which is consistent with its heavy mineral composition (ca. 10% zircon compared to ca. 1% in the upstream sample, Table 2). Consequently, the downstream Fitzroy River data are assumed to represent the fingerprint of proximal recycling. For instance, Alice Springs Orogeny-derived detritus may be sourced from sedimentary rocks within the catchment of the Fitzroy River, such as the exposed Permian Grant Group (Martin et al., 2019). As the proximal recycling fingerprint somewhat differs from the Broome Sandstone (Figure 3), contributions from other sources can be inferred.

The influence of extra-basinal recycling on the Broome Sandstone detrital record can also be addressed by comparing the bivariate U–Pb and Lu–Hf composition of its detrital zircon to data from potential intermediate sediment sources. Volumetrically significant sedimentary basins that border the Canning Basin represent viable sediment sources as they reveal highly similar detrital zircon U–Pb and Hf values to those of the Broome Sandstone (Figure 7). For instance, the Amadeus Basin, which hosts Arunta region detritus (right Amadeus Basin envelope in Figure 7) has striking similarity to the ca. 1690–1430 Ma age mode of the Broome Sandstone. Generally, high similarity to possible intermediate sources (mainly Amadeus and Officer basins), compared to ultimate crystalline sources (Figure 7), implies sediment transport of recycled grains from central Australian basins. This correlation between the Broome Sandstone and the central Australian sediments, as well as a difference to other intermediate source areas (e.g., Yeneena Basin; Figure 2b), is indicated by statistical comparison. Bivariate MDS (U–Pb and Hf of detrital zircon) of potential intermediate sources highlight similarity of the Broome Sandstone detritus to samples from the Amadeus, Officer and Murraba basins. Those basins contain high abundances of Arunta region- and Musgrave Province-derived detrital zircon and are interpreted as major sources of recycled zircon grains for the Broome Sandstone. This proposed recycling relationship is consistent with (i) a lower median α-dose value (a proxy for sedimentary recycling and/or transport; e.g., Dröllner et al., 2022; Markwitz & Kirkland, 2018) of the Broome Sandstone compared to the Amadeus Basin (Figure S6) and (ii) the relatively high degree (ca. 50%) of discordant zircon grains. Similarly, about 62% of the rutile analyses show elevated Th contents, which is unusual for primary metamorphic rutile (Zack et al., 2011), perhaps suggesting secondary overprinting consistent with a multi-cycle origin for a significant portion of the rutile grains. However, the disturbance of zircon and rutile U–Pb systems can also be explained by the polyphase geological histories of the inferred ultimate crystalline source areas. The inferred Broome Sandstone sediment sourcing from Neoproterozoic basins, which were deposited prior to the Alice Springs Orogeny (ca. 450–300 Ma; Buick et al., 2008), is supported by low numbers of detrital zircon and rutile ages (within the Broome Sandstone) corresponding to the timing of the Alice Springs Orogeny (Figure 3). Such ages are observed in some sediments of the Canning Basin (e.g., Grant Group; Martin et al., 2019) but would have been absent in Neoproterozoic basins (e.g., Amadeus Basin; Haines et al., 2016). The Officer Basin at the southwestern fringes of the Canning Basin is largely covered by sediments and hence is not expected to directly shed detritus into the Canning Basin during the Cretaceous, which is consistent with an absence of characteristic primary detritus shedding from the west, as discussed in the previous section. Ultimately, central Australian sedimentary basins peripheral to the Canning Basin are, in tandem with central Australian basement rocks, considered the most likely sources of Lower Cretaceous sediments.

5.3 | Out of central Australia—Sediment generation and continental drainage

The source-to-sink correlations suggest an Early Cretaceous sediment routing system originating in central Australia and transporting detritus northwestwards. The distance between the sink (Broome Sandstone) and the inferred source area of most detrital zircon and rutile (central Australian Musgrave Province and Arunta region including adjacent sedimentary basins) is some 1000 km. This distance implies a large-scale drainage system. The detailed extent of the drainage system that is the source of the fluvio-deltaic sediments of the Broome Sandstone remains speculative. However, a channelized route along the central NW-trending Canning Basin, with subordinate tributaries feeding sediments from the west and the northeastern parts of the basin borders, is envisaged to explain the observed central Australian source signal, as well as minor intrabasinal sediment recycling during fluvial transport. This is consistent with highly polymodal detrital zircon and rutile age spectra implying extensive transport and mixing of different detritus. Additional support for a large-scale drainage system with headwaters in central Australia

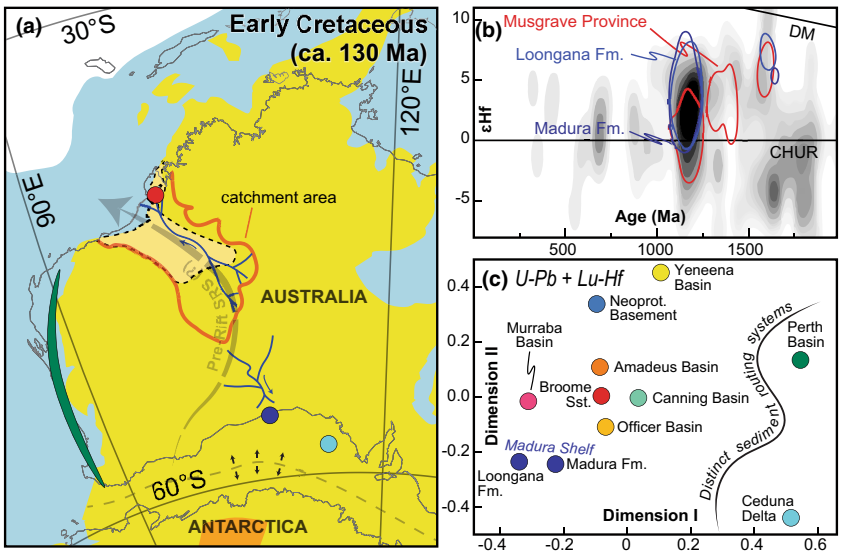

FIGURE 11 (a) Schematic paleogeographic interpretation of the broader catchment and principal sediment routing of the Lower Cretaceous Broome Sandstone after the termination of a pre-rift routing system. SRS, sediment routing system. Colour-coded circles and ellipses show location of reference data in (c). (b) Close-up of the Hf isotope compositions of concordant detrital zircon from the Broome Sandstone (samples THB001, THB002 and THB003; grey bivariate kernel density estimate; see Figure 4) and 75% peak density contours (Figure 7) of the Lower Cretaceous Madura and Loongana formations (Barham et al., 2018), and Musgrave Province (Kirkland, Smithies, et al., 2013). DM and CHUR values after Griffin et al. (2000) and Bouvier et al. (2008), respectively. (c) Bivariate multidimensional scaling of concordant detrital zircon using U–Pb and Lu–Hf data of the Broome Sandstone and literature data. References: Ceduna Delta—Lloyd et al. (2016); Madura Shelf—Barham et al. (2018); Perth Basin—Olierook et al. (2019) and references therein. Remaining references are provided in Figures 4, 10 and Table S3.

can be deduced from the detrital signature of the downstream Fitzroy River sample (FIT001). The Fitzroy River terminates in a similar position but has a significantly smaller catchment than the interpreted Early Cretaceous sediment routing system. As mentioned above, the age spectra in the downstream sediments are controlled by sediment recycling. Despite this, the downstream sample shows, compared to the Broome Sandstone, more ages corresponding to the Hooper Orogeny (exposed in the eastern and central Lamboo Province; Tyler et al., 2012) and the Alice Springs Orogeny (occurring in proximal Permian and Triassic strata, Figure 9). Such nuanced indications of local sediment shedding are not pronounced in the Broome Sandstone age spectra, which is rather dominated by distal source signatures that potentially diluted the detrital record of volumetrically insignificant source areas.

Contextualization of this interpreted northwestward-shedding sediment routing system with literature data suggests that a Cretaceous drainage divide is located in central Australia. Essentially contemporaneous deposits on the Madura Shelf in southern Australia show a pronounced dominance of Mesoproterozoic detrital zircon grains consistent with sediment routing from the Musgrave Province (Barham et al., 2018). This suggests coeval north- and southward sediment transport from central Australia (Figure 11a). The distinctive central Australian source signal (Figure 11b) of the southward shedding system is interpreted to reflect isolation from other sedimentary systems, for example the easterly located Cretaceous Ceduna Delta in South Australia (Figure 11; Barham et al., 2018). Likewise, the northward sediment transfer is distinct to the westerly located Perth Basin, based on U–Pb and Hf isotopic data of detrital zircon (Figure 11c). Additionally, eastward shedding of central Australian detrital cargo is interpreted based on mineralogical and geochemical data of Lower Cretaceous sedimentary rocks in parts of the Eromanga Basin (Baudet et al., 2021). Collectively, such observations imply that central Australia, especially the Musgrave Province and the Arunta region (including their sedimentary cover), had a vital role for sediment generation and likely acted as a major drainage divide during the Lower Cretaceous.

5.4 | Controls and implications of the post-Gondwanan reorganization of continent-scale sediment routing

The widespread and prolonged occurrence of central Australian-, and specifically Musgrave Province-derived signatures (Figure 9), is likely controlled by tectonic processes. Importantly, central Australian detritus has also been widely recognized in pre-Cretaceous strata throughout Australia (e.g., Haines et al., 2016; Keeman et al., 2020;

Verdel et al., 2021). The detrital record of the denudation and transport of Musgrave Province material is witnessed in sediments as distal as the Adelaide Rift Complex in South Australia (Haines et al., 2004; Keeman et al., 2020) and the Charters Towers Province in Queensland (Haines et al., 2016). The initiation of widespread shedding of ultimate Musgrave Province detritus has been related to uplift and erosion of the Musgrave Province rocks and associated sedimentary basins, a response to the ca. 600–530 Ma Petermann Orogeny (Haines et al., 2016; Raimondo et al., 2014; Wade et al., 2006). However, uplift of Musgrave Province may have commenced significantly earlier at ca. 750–720 Ma (Camacho et al., 2002; Howard et al., 2015; Quentin de Gromard et al., 2019). This first phase of shedding of central Australian detritus was followed by a second phase, corresponding to the Alice Springs Orogeny, and resulting in uplift and significant denudation of central Australian lithologies (Hand & Sandiford, 1999; Raimondo et al., 2014). Combining these orogenic and some minor tectonic events, a protracted geological history of intracontinental tectonic activity, that exceeds 700 Myr, can be reconstructed for central Australia (Quentin de Gromard et al., 2019). Consequently, tectonic activity generating topographic relief within the catchment is likely controlling a prolonged headward erosion in central Australia. Thus, the observed depositional response to a long-lived drainage system with headwaters in central Australia may have been driven by preferential erosion (Cawood et al., 2003; Spencer et al., 2018). This effect may have been intensified by relatively high Zr contents, hence high zircon fertility, of granitoids of the Musgrave Province (e.g., Howard et al., 2015). The existence of sufficient relief during the Early Cretaceous is consistent with paleo-topography modelling results (Braz et al., 2021). Ultimately, the Lower Cretaceous drainage system forms part of a sediment dispersal network carrying a central Australian signature. The dispersion of this signal, either directly (first-cycle) or indirectly (multi-cycle), remains active until the present. This is as exemplified by the dominance of Musgrave Province detritus, which is likely sourced via sedimentary recycling, in modern beach sands near Broome (Figures 2a and 3).

Similarities in provenance proxy characters throughout the Canning Basin sediments (Figure 9) suggests a long-lived sediment routing system with an extensive catchment. Part of this catchment may have been in Antarctica (Morón et al., 2019). However, establishing direct fluvial connections within this continental catchment remains ambiguous due to widespread occurrence of potential intermediate reservoirs of Antarctic detritus within sedimentary basins (Kirkland et al., 2020). These intermittent sources of recycled detritus are fertile hosts of polymodal detrital age signatures, some akin to those used to infer a direct source (Figure 7). Thus, indirect sourcing (via sediment recycling) remains a possible alternative that demands additional tools to refine source-to-sink correlations such as (U-Th)/He thermochronology of detrital zircon (e.g., Rahl et al., 2003), Pb isotopes in feldspar (e.g., Tyrrell et al., 2009), and geochronology of diagenetic phases (e.g., Moecher et al., 2019). Integration of such tools may also help to overcome the remaining ambiguity around source-to-sink correlations of this work, which is well-illustrated by the challenging discrimination of several potential source terranes despite the multi-proxy approach used (e.g., overlapping source Hf envelops in Figure 7). Some challenges may also derive from a paucity of multi-proxy information of crystalline sources (e.g., trace element data) to facilitate comparison of source and sink. However, the lack of multi-proxy reference data for important source areas may be resolved via the study of modern catchments to fingerprint these sources as demonstrated by the integration of the modern Fitzroy River sediments.

Provenance constraints of the Canning Basin in tandem with the tectonic history of central Australia suggest that the lower Cretaceous sediment routing system followed a pre-existing sedimentary pathway. Such sediment routing of central Australian detrital cargo has been previously suggested to be a subsidiary system during Gondwanan times (Morón et al., 2019). Consequently, post-Gondwana drainage reorganization, after the rift initiation between Australia and Antarctica, is expressed in the persistence and isolation of a northward draining system. Dissection of paleo-drainages has also been recognized in other sedimentary systems, such as the paleo-Yangtze drainage system (Zhang, Tyrrell, et al., 2014). This suggests that established pathways, maybe as remnants of larger continental drainage systems, may control subsequent sediment routes. Furthermore, central Australia's long-lived history of sediment generation provides a further instance of a drainage system chiefly controlled by external forcing. Similarly, other examples of persistent drainage systems are inferred to be the result of topographic uplift associated with deeper processes (e.g., Castelltort et al., 2012; Chardon et al., 2016; Faccenna et al., 2019; Maselli et al., 2020). Collectively, this highlights the importance of deep-rooted geological processes on the evolution of sedimentary routing systems.

6 | CONCLUSIONS

The presented work uses a multi-proxy approach analysing detrital zircon (U–Pb, Lu–Hf and trace elements) and rutile (U–Pb and trace elements) from the Lower Cretaceous Broome Sandstone of the Canning Basin (NW Australia) and proximal modern sediments. The results

are used to reconstruct the dominant sediment routing system and its controls. Key conclusions are as follows:

- The use of the mineral pair zircon-rutile integrated with multiple (isotope) geochemical proxies improves source-to-sink correlation. Specifically, this approach improves discrimination of source rocks within the intracratonic Canning Basin that is bordered by crystalline basement lithologies of broadly coeval Proterozoic age. Furthermore, contextualization with modern fluvial sediments is helpful in resolving the detrital fingerprint of possible ultimate and intermediate source areas. However, some ambiguity for certain source areas remains and demands assessment of additional tools, particularly to improve discrimination of first- and multi-cycle detritus.
- The detrital record of the Lower Cretaceous Broome Sandstone corresponds to an ultimate crystalline provenance of central Australian lithologies, mainly those allied to the Musgrave Province and the Arunta region. Based on strong similarity to Broome Sandstone detritus, intermediate sedimentary sources within central Australia (e.g., Amadeus Basin) are interpreted as a key source of multi-cycle detritus that potentially exceed first-cycle detritus.
- On the basis of the established source-to-sink correlation, a sediment routing system with headwaters in central Australia is inferred. This system represents large-scale drainage that effectively diluted the detrital record of proximal sediment input. A review of other Cretaceous sediment routing systems suggests widespread shedding of central Australian detrital signatures, mainly corresponding to Musgrave Province detritus. Therefore, central Australia was likely fundamental for sediment generation and acted as a major drainage divide during the Early Cretaceous.
- Extensive intrabasinal recycling of pre-Cretaceous Canning Basin strata represents an alternative interpretation of the observed detrital signatures. However, a more likely explanation is that erosion and denudation of central Australian lithologies was driven by the prolonged intracontinental tectonic activity of central Australia. Ultimately, this external forcing created the necessary relief for near-continuous denudation, establishing a long-lived sediment drainage network situated in central Australia.
- Results indicate that the post-Gondwanan drainage is established on the basis of pre-existing sediment pathways. Such pathways provided a template for the sedimentary reorganization after supercontinent dispersal.

ACKNOWLEDGEMENTS

This research was supported by MRIWA grant M551 and received further financial support from The Institute for Geoscience Research (TIGeR; Curtin University). We are thankful to the Yawuru community for access to their land (Gantheaume Point) during fieldwork, which has been kindly supported by the Shire of Broome. We thank Rohan Hine and David Sleigh of Iluka Resources for discussions. We thank Seb Grey and Sheffield Resources for discussions and provision of samples. We also would like to thank Maike Schulz for assisting with fieldwork, and Noreen Evans and Brad McDonald for help with LA-ICP-MS analysis. This work greatly benefited from editorial handling by Cari Johnson and journal reviews by Peter Haines and two anonymous reviewers. Part of this research was undertaken using electron microscope instrumentation (ARC LE190100176 & LE140100150) at the John de Laeter Centre (JdLC), Curtin University. Research in the GeoHistory Facility, JdLC is enabled by AuScope (auscope.org.au) and the Australian Government via the National Collaborative Research Infrastructure Strategy (NCRIS). The NPII multi-collector was obtained via funding from the Australian Research Council LIEF programme (LE150100013). Open access is made available through the Read & Publish agreement of Wiley and the Council of Australian University Librarians.

CONFLICT OF INTEREST

The authors have declared no conflicts of interest for this article.

PEER REVIEW

The peer review history for this article is available at https://publons.com/publon/10.1111/bre.12715.

DATA AVAILABILITY STATEMENT

The data that support the findings of this study are available in Supporting Information S1 (Analytical procedures, Figures S1–S6, and Table S3) and Supporting Information S2 (Tables S1 and S2).

ORCID

Maximilian Dröllner https://orcid.org/0000-0001-8661-9565
Milo Barham https://orcid.org/0000-0003-0392-7306
Christopher L. Kirkland https://orcid.org/0000-0003-3367-8961

REFERENCES

Armitage, J. J., Duller, R. A., Whittaker, A. C., & Allen, P. A. (2011). Transformation of tectonic and climatic signals from source to sedimentary archive. *Nature Geoscience*, *4*, 231–235.

Aubrecht, R., Sýkora, M., Uher, P., Li, X.-H., Yang, Y.-H., Putiš, M., & Plašienka, D. (2017). Provenance of the Lunz Formation (Carnian) in the Western Carpathians, Slovakia: Heavy mineral study and in situ LA–ICP–MS U–Pb detrital zircon dating. *Palaeogeography, Palaeoclimatology, Palaeoecology*, *471*, 233–253.

Auchter, N. C., Romans, B. W., Hubbard, S. M., Daniels, B. G., Scher, H. D., & Buckley, W. (2020). Intrabasinal sediment recycling

from detrital strontium isotope stratigraphy. *Geology*, *48*, 992–996.

Bagas, L. (2004). Proterozoic evolution and tectonic setting of the Northwest Paterson Orogen, Western Australia. *Precambrian Research*, *128*, 475–496.

Bagas, L., Anderson, J., & Bierlein, F. P. (2009). Palaeoproterozoic evolution of the Killi Formation and orogenic gold mineralization in the Granites–Tanami Orogen, Western Australia. *Ore Geology Reviews*, *35*, 47–67.

Barham, M., & Kirkland, C. L. (2020). Changing of the guards: Detrital zircon provenance tracking sedimentological reorganization of a post-Gondwanan rift margin. *Basin Research*, *32*, 854–874.

Barham, M., Reynolds, S., Kirkland, C. L., O'Leary, M. J., Evans, N. J., Allen, H. J., Haines, P. W., Hocking, R. M., & McDonald, B. J. (2018). Sediment routing and basin evolution in Proterozoic to Mesozoic East Gondwana: A case study from southern Australia. *Gondwana Research*, *58*, 122–140.

Baudet, E., Tiddy, C., Giles, D., Hill, S., & Gordon, G. (2021). Diverse provenance of the lower cretaceous sediments of the Eromanga Basin, South Australia: Constraints on basin evolution. *Australian Journal of Earth Sciences*, *68*, 316–342.

Belousova, E., Griffin, W., O'Reilly, S. Y., & Fisher, N. (2002). Igneous zircon: Trace element composition as an indicator of source rock type. *Contributions to Mineralogy and Petrology*, *143*, 602–622.

Belousova, E. A., Kostitsyn, Y. A., Griffin, W. L., Begg, G. C., O'Reilly, S. Y., & Pearson, N. J. (2010). The growth of the continental crust: Constraints from zircon Hf-isotope data. *Lithos*, *119*, 457–466.

Blum, M., & Pecha, M. (2014). Mid-cretaceous to Paleocene north American drainage reorganization from detrital zircons. *Geology*, *42*, 607–610.

Blum, M., Rogers, K., Gleason, J., Najman, Y., Cruz, J., & Fox, L. (2018). Allogenic and autogenic signals in the stratigraphic record of the Deep-Sea Bengal fan. *Scientific Reports*, *8*, 7973.

Bodorkos, S., 2011, *Geoscience Australia's Geochron delivery system* (first release: September 2011). Geoscience Australia. http://pid.geoscience.gov.au/dataset/ga/72841.

Bodorkos, S., Oliver, N. H. S., & Cawood, P. A. (1999). Thermal evolution of the central Halls Creek Orogen, northern Australia. *Australian Journal of Earth Sciences*, *46*, 453–465.

Bouvier, A., Vervoort, J. D., & Patchett, P. J. (2008). The Lu–Hf and Sm–Nd isotopic composition of CHUR: Constraints from unequilibrated chondrites and implications for the bulk composition of terrestrial planets. *Earth and Planetary Science Letters*, *273*, 48–57.

Boyd, D. M., & Teakle, M. G. (2016). Thunderbird heavy mineral sand deposit, Western Australia. *Applied Earth Science*, *125*, 128–139.

Bracciali, L. (2019). Coupled zircon-rutile U-Pb chronology: LA ICP-MS dating, geological significance and applications to sediment provenance in the eastern Himalayan-indo-Burman region. *Geosciences*, *9*, 467.

Braz, C., Zahirovic, S., Salles, T., Flament, N., Harrington, L., & Müller, R. D. (2021). Modelling the role of dynamic topography and eustasy in the evolution of the great Artesian Basin. *Basin Research*, *33*, 3378–3405. https://doi.org/10.1111/bre.12606

Buick, I. S., Storkey, A., & Williams, I. S. (2008). Timing relationships between pegmatite emplacement, metamorphism and deformation during the intra-plate Alice Springs Orogeny, Central Australia. *Journal of Metamorphic Geology*, *26*, 915–936.

Camacho, A., Hensen, B. J., & Armstrong, R. (2002). Isotopic test of a thermally driven intraplate orogenic model, Australia. *Geology*, *30*, 887.

Cao, W., Zahirovic, S., Flament, N., Williams, S., Golonka, J., & Müller, R. D. (2017). Improving global paleogeography since the late Paleozoic using paleobiology. *Biogeosciences*, *14*, 5425–5439.

Cassidy, K. F., Champion, D. C., Krapez, B., Barley, M. E., Brown, S. J., Blewett, R. S., Groenewald, P. B., & Tyler, I. M. (2006). A revised geological framework for the Yilgarn Craton, Western Australia. *Geological Survey of Western Australia, Record*, *8*(8), 15.

Castelltort, S., Goren, L., Willett, S. D., Champagnac, J.-D., Herman, F., & Braun, J. (2012). River drainage patterns in the New Zealand Alps primarily controlled by plate tectonic strain. *Nature Geoscience*, *5*, 744–748.

Cawood, P. A., & Nemchin, A. A. (2000). Provenance record of a rift basin: U/Pb ages of detrital zircons from the Perth Basin, Western Australia. *Sedimentary Geology*, *134*, 209–234.

Cawood, P. A., Nemchin, A. A., Freeman, M., & Sircombe, K. (2003). Linking source and sedimentary basin: Detrital zircon record of sediment flux along a modern river system and implications for provenance studies. *Earth and Planetary Science Letters*, *210*, 259–268.

Cawood, P. A., & Tyler, I. M. (2004). Assembling and reactivating the Proterozoic Capricorn Orogen: Lithotectonic elements, orogenies, and significance. *Precambrian Research*, *128*, 201–218.

Champion, D. C., & Smithies, R. H. (2007). Chapter 4.3 geochemistry of Paleoarchean granites of the east Pilbara terrane, Pilbara Craton, Western Australia: Implications for early Archean crustal growth. In M. J. van Kranendonk, R. H. Smithies, & V. C. Bennett (Eds.), *Developments in Precambrian geology Earth's oldest rocks* (pp. 369–409). Elsevier.

Chardon, D., Grimaud, J.-L., Rouby, D., Beauvais, A., & Christophoul, F. (2016). Stabilization of large drainage basins over geological time scales: Cenozoic West Africa, hot spot swell growth, and The Niger River. *Geochemistry, Geophysics, Geosystems*, *17*, 1164–1181.

Cherniak, D. J. (2000). Pb diffusion in rutile. *Contributions to Mineralogy and Petrology*, *139*(2), 198–207. https://doi.org/10.1007/pl00007671

Cherniak, D., & Watson, E. (2001). Pb diffusion in zircon. *Chemical Geology*, *172*, 5–24.

Chew, D., O'Sullivan, G., Caracciolo, L., Mark, C., & Tyrrell, S. (2020). Sourcing the sand: Accessory mineral fertility, analytical and other biases in detrital U-Pb provenance analysis. *Earth-Science Reviews*, *202*, 103093.

Clark, M. K., Schoenbohm, L. M., Royden, L. H., Whipple, K. X., Burchfiel, B. C., Zhang, X., Tang, W., Wang, E., & Chen, L. (2004). Surface uplift, tectonics, and erosion of eastern Tibet from large-scale drainage patterns. *Tectonics*, *23*, TC1006. https://doi.org/10.1029/2002TC001402

Collins, W. (1995). Geochronological constraints on orogenic events in the Arunta inlier: A review. *Precambrian Research*, *71*, 315–346.

Collins, W. J., Belousova, E. A., Kemp, A. I. S., & Murphy, J. B. (2011). Two contrasting Phanerozoic orogenic systems revealed by hafnium isotope data. *Nature Geoscience*, *4*, 333–337.

Crossman, S., & Li, O. (2015). Surface hydrology lines (regional). Geoscience Australia. http://pid.geoscience.gov.au/dataset/ga/83107

Davis, S. J., Dickinson, W. R., Gehrels, G. E., Spencer, J. E., Lawton, T. F., & Carroll, A. R. (2010). The Paleogene California River: evidence of Mojave-Uinta paleodrainage from U-Pb ages of detrital zircons. *Geology*, *38*, 931–934.

Direen, N. G. (2011). Comment on "Antarctica—Before and after Gondwana" by SD Boger Gondwana Research, Volume 19, Issue 2, March 2011, Pages 335–371. *Gondwana Research*, *21*(1), 302–304.

Dröllner, M., Barham, M., & Kirkland, C. L. (2022). Gaining from loss: Detrital zircon source-normalized α-dose discriminates first- versus multi-cycle grain histories. *Earth and Planetary Science Letters*, *579*, 117346.

Dumitru, T. A. (2016). A new zircon concentrating table designed for geochronologists. In *AGU Fall Meeting Abstracts* (Vol. *2016*, pp. V23A–V2956A). American Geophysical Union.

Eriksson, K. A., Campbell, I. H., Palin, J. M., Allen, C. M., & Bock, B. (2004). Evidence for multiple recycling in Neoproterozoic through Pennsylvanian sedimentary rocks of the central Appalachian Basin. *The Journal of Geology*, *112*, 261–276.

Faccenna, C., Glišović, P., Forte, A., Becker, T. W., Garzanti, E., Sembroni, A., & Gvirtzman, Z. (2019). Role of dynamic topography in sustaining the Nile River over 30 million years. *Nature Geoscience*, *12*, 1012–1017.

Force, E. R. (1980). The provenance of rutile. *Journal of Sedimentary Petrology*, *50*, 485–488.

Forman, D. J., & Wales, D. W. (1981). *Geological evolution of the Canning Basin, Western Australia*. Canberra, Bureau of Mineral Resources, Geology, and Geophysics.

Gardiner, N. J., Kirkland, C. L., & van Kranendonk, M. J. (2016). The juvenile hafnium isotope signal as a record of supercontinent cycles. *Scientific Reports*, *6*, 38503.

Gardiner, N. J., Maidment, D. W., Kirkland, C. L., Bodorkos, S., Smithies, R. H., & Jeon, H. (2018). Isotopic insight into the Proterozoic crustal evolution of the Rudall Province, Western Australia. *Precambrian Research*, *313*, 31–50.

Gibbons, A. D., Whittaker, J. M., & Müller, D. R. (2013). The breakup of East Gondwana: Assimilating constraints from cretaceous ocean basins around India into a best-fit tectonic model: Journal of geophysical research. *Solid Earth*, *118*, 808–822.

Gillespie, J., Glorie, S., Khudoley, A., & Collins, A. S. (2018). Detrital apatite U-Pb and trace element analysis as a provenance tool: Insights from the Yenisey ridge (Siberia). *Lithos*, *314-315*, 140–155.

Griffin, W. L., Pearson, N. J., Belousova, E., Jackson, S. E., van Achterbergh, E., O'Reilly, S. Y., & Shee, S. R. (2000). The Hf isotope composition of cratonic mantle: LAM-MC-ICPMS analysis of zircon megacrysts in kimberlites. *Geochimica et Cosmochimica Acta*, *64*, 133–147.

Grimes, C. B., John, B. E., Kelemen, P. B., Mazdab, F. K., Wooden, J. L., Cheadle, M. J., Hanghøj, K., & Schwartz, J. J. (2007). Trace element chemistry of zircons from oceanic crust: A method for distinguishing detrital zircon provenance. *Geology*, *v. 35*, 643.

Grimes, C. B., Wooden, J. L., Cheadle, M. J., & John, B. E. (2015). "Fingerprinting" tectono-magmatic provenance using trace elements in igneous zircon. *Contributions to Mineralogy and Petrology*, *170*, 1–26.

Haines, P. W., Kirkland, C. L., Wingate, M., Allen, H., Belousova, E. A., & Gréau, Y. (2016). Tracking sediment dispersal during orogenesis: A zircon age and Hf isotope study from the western Amadeus Basin, Australia. *Gondwana Research*, *37*, 324–347.

Haines, P. W., Turner, S. P., Kelley, S. P., Wartho, J.-A., & Sherlock, S. C. (2004). ^{40}Ar–^{39}Ar dating of detrital muscovite in provenance investigations: A case study from the Adelaide rift complex, South Australia. *Earth and Planetary Science Letters*, *227*, 297–311.

Haines, P. W., & Wingate, M. T. D. (2007). Fingerprinting reservoir sandstone provenance in the Canning Basin using detrital zircons: Geological survey of Western Australia. *Annual Review*, 2005–2006. https://dmpbookshop.eruditetechnologies.com.au/product/fingerprinting-reservoir-sandstone-provenance-in-the-canning-basin-using-detrital-zircons.do

Haines, P. W., Wingate, M. T. D., & Kirkland, C. L. (2013). Detrital zircon U-Pb ages from the paleozoic of the canning and officer basins, Western Australia: Implications for provenance and interbasin connections. In *West Australian basins symposium* (p. 19). Petroleum Exploration Society of Australia.

Haines, P. W., Wingate, M. T. D., Zhang, Y., & Maidment, D. W. (2018). Looking beneath the Canning Basin: New insights from geochronology, seismic and potential-field data. *GSWA Extended Abstracts*, *2018*, 4.

Hand, M., & Sandiford, M. (1999). Intraplate deformation in Central Australia, the link between subsidence and fault reactivation. *Tectonophysics*, *v. 305*, 121–140.

Hashimoto, T., Bailey, A., Chirinos, A., & Carr, L. K. (2018). *Onshore basin inventory volume 2: The canning, Perth and Officer basins* (p. 125). Geoscience Australia.

Hickman, A. H., & van Kranendonk, M. J. (2012). Early earth evolution: Evidence from the 3.5–1.8 Ga geological history of the Pilbara region of Western Australia. *Episodes*, *35*, 283–297.

Hollis, J. A., Kemp, A. I. S., Tyler, I. M., Kirkland, C. L., Wingate, M. T. D., Phillips, C., Sheppard, S., Belousova, E., & Gréau, Y. (2014). Basin formation by orogenic collapse: Zircon U-Pb and Lu-Hf isotope evidence from the Kimberley and Speewah groups, northern Australia. *Report*, *137*.

Hollis, J. A., Kirkland, C. L., Spaggiari, C. V., Tyler, I. M., Haines, P. W., Wingate, M. T. D., Belousova, E. A., & Murphy, R. C. (2013). Zircon U–Pb–Hf isotope evidence for links between the Warumpi and aileron provinces, west Arunta region: GSWA. *Record*, *9*.

Hoskin, P. W., & Ireland, T. R. (2000). Rare earth element chemistry of zircon and its use as a provenance indicator. *Geology*, *28*, 627.

Howard, H. M., Smithies, R. H., Kirkland, C. L., Kelsey, D. E., Aitken, A., Wingate, M., Quentin de Gromard, R., Spaggiari, C. V., & Maier, W. D. (2015). The burning heart—The Proterozoic geology and geological evolution of the west Musgrave Region, central Australia. *Gondwana Research*, *27*, 64–94.

Howard, K. E., Hand, M., Barovich, K. M., Reid, A., Wade, B. P., & Belousova, E. A. (2009). Detrital zircon ages: Improving interpretation via Nd and Hf isotopic data. *Chemical Geology*, *262*, 277–292.

Johnson, S. P., Korhonen, F. J., Kirkland, C. L., Cliff, J. B., Belousova, E. A., & Sheppard, S. (2017). An isotopic perspective on growth and differentiation of Proterozoic orogenic crust: From subduction magmatism to cratonization. *Lithos*, *268-271*, 76–86.

Keeman, J., Turner, S., Haines, P. W., Belousova, E., Ireland, T., Brouwer, P., Foden, J., & Wörner, G. (2020). New U Pb, Hf and O isotope constraints on the provenance of sediments from the Adelaide rift complex – Documenting the key Neoproterozoic to early Cambrian succession. *Gondwana Research*, *83*, 248–278.

Kirkland, C. L., Barham, M., & Danišík, M. (2020). Find a match with triple-dating: Antarctic sub-ice zircon detritus on the modern shore of Western Australia. *Earth and Planetary Science Letters*, *531*, 115953.

Kirkland, C. L., Johnson, S. P., Smithies, R. H., Hollis, J. A., Wingate, M., Tyler, I. M., Hickman, A. H., Cliff, J. B., Tessalina, S., Belousova, E. A., & Murphy, R. C. (2013). Not-so-suspect terrane: Constraints on the crustal evolution of the Rudall Province. *Precambrian Research*, *235*, 131–149.

Kirkland, C. L., Smithies, R. H., Woodhouse, A. J., Howard, H. M., Wingate, M. T., Belousova, E. A., Cliff, J. B., Murphy, R. C., & Spaggiari, C. V. (2013). Constraints and deception in the isotopic record; the crustal evolution of the west Musgrave Province, central Australia. *Gondwana Research*, *v. 23*, 759–781.

Kirkland, C. L., Spaggiari, C. V., Pawley, M. J., Wingate, M., Smithies, R. H., Howard, H. M., Tyler, I. M., Belousova, E. A., & Poujol, M. (2011). On the edge: U–Pb, Lu–Hf, and Sm–Nd data suggests reworking of the Yilgarn Craton margin during formation of the Albany-Fraser Orogen. *Precambrian Research*, *187*, 223–247.

Kohn, M. J., Corrie, S. L., & Markley, C. (2015). The fall and rise of metamorphic zircon. *American Mineralogist*, *100*, 897–908.

Krippner, A., & Bahlburg, H. (2013). Provenance of Pleistocene Rhine River middle terrace sands between the Swiss–German border and Cologne based on U–Pb detrital zircon ages. *International Journal of Earth Sciences*, *102*, 917–932.

Lloyd, J., Collins, A. S., Payne, J. L., Glorie, S., Holford, S., & Reid, A. J. (2016). Tracking the cretaceous transcontinental Ceduna River through Australia: The hafnium isotope record of detrital zircons from offshore southern Australia. *Geoscience Frontiers*, *7*, 237–244.

Ludwig, K. R. (1998). On the treatment of concordant uranium-Lead ages. *Geochimica et Cosmochimica Acta*, *62*, 665–676.

Maidment, D. W., Williams, I. S., & Hand, M. (2007). Testing long-term patterns of basin sedimentation by detrital zircon geochronology, Centralian Superbasin, Australia. *Basin Research*, *19*, 335–360.

Malkowski, M. A., Sharman, G. R., Johnstone, S. A., Grove, M. J., Kimbrough, D. L., & Graham, S. A. (2019). Dilution and propagation of provenance trends in sand and mud: Geochemistry and detrital zircon geochronology of modern sediment from Central California (U.S.A.). *American Journal of Science*, *319*, 846–902.

Malusà, M. G., Resentini, A., & Garzanti, E. (2016). Hydraulic sorting and mineral fertility bias in detrital geochronology. *Gondwana Research*, *31*, 1–19.

Markwitz, V., & Kirkland, C. L. (2018). Source to sink zircon grain shape: Constraints on selective preservation and significance for Western Australian Proterozoic basin provenance. *Geoscience Frontiers*, *9*(2), 415–430. https://doi.org/10.1016/j.gsf.2017.04.004

Martin, E. L., Collins, W. J., & Kirkland, C. L. (2017). An Australian source for Pacific-Gondwanan zircons: Implications for the assembly of northeastern Gondwana. *Geology*, *45*, G39152.1.

Martin, J. R., Redfern, J., Horstwood, M. S. A., Mory, A. J., & Williams, B. P. J. (2019). Detrital zircon age and provenance constraints on late Paleozoic ice-sheet growth and dynamics in Western and Central Australia. *Australian Journal of Earth Sciences*, *66*, 183–207.

Maselli, V., Kroon, D., Iacopini, D., Wade, B. S., Pearson, P. N., & de Haas, H. (2020). Impact of the east African rift system on the routing of the deep-water drainage network offshore Tanzania, western Indian Ocean. *Basin Research*, *32*, 789–803.

Meinhold, G., Anders, B., Kostopoulos, D., & Reischmann, T. (2008). Rutile chemistry and thermometry as provenance indicator: An example from Chios Island, Greece. *Sedimentary Geology*, *203*, 98–111.

Moecher, D. P., Kelly, E. A., Hietpas, J., & Samson, S. D. (2019). Proof of recycling in clastic sedimentary systems from textural analysis and geochronology of detrital monazite: Implications for detrital mineral provenance analysis. *Bulletin*, *131*, 1115–1132.

Moecher, D. P., & Samson, S. D. (2006). Differential zircon fertility of source terranes and natural bias in the detrital zircon record: Implications for sedimentary provenance analysis. *Earth and Planetary Science Letters*, *247*, 252–266.

Mole, D. R., Kirkland, C. L., Fiorentini, M. L., Barnes, S. J., Cassidy, K. F., Isaac, C., Belousova, E. A., Hartnady, M., & Thebaud, N. (2019). Time-space evolution of an Archean craton: A Hf-isotope window into continent formation. *Earth-Science Reviews*, *196*, 102831.

Morón, S., Cawood, P. A., Haines, P. W., Gallagher, S. J., Zahirovic, S., Lewis, C. J., & Moresi, L. (2019). Long-lived transcontinental sediment transport pathways of East Gondwana. *Geology*, *47*, 513–516.

Morón, S., Kohn, B. P., Beucher, R., Mackintosh, V., Cawood, P. A., Moresi, L., & Gallagher, S. J. (2020). Denuding a craton: Thermochronology record of Phanerozoic unroofing from the Pilbara Craton, Australia. *Tectonics*, *39*, e2019TC005988.

Morton, A. C., & Hallsworth, C. R. (1999). Processes controlling the composition of heavy mineral assemblages in sandstones. *Sedimentary Geology*, *124*, 3–29.

Mory, A. J., & Hocking, R. M. (2011). *Permian, carboniferous and upper devonian geology of the Northern Canning Basin, Western Australia: A field guide*. Geological Survey of Western Australia.

Müller, R. D., Cannon, J., Qin, X., Watson, R. J., Gurnis, M., Williams, S., Pfaffelmoser, T., Seton, M., Russell, S. H. J., & Zahirovic, S. (2018). GPlates: Building a virtual earth through deep time. *Geochemistry, Geophysics, Geosystems*, *19*, 2243–2261.

Nelson, D. R. (2004). 169034: biotite monzogranite, Ripon Hills Road - Talga River crossing. *Geochronology Record*, *151*.

Olierook, H. K., Barham, M., Fitzsimons, I. C., Timms, N. E., Jiang, Q., Evans, N. J., & McDonald, B. J. (2019). Tectonic controls on sediment provenance evolution in rift basins: Detrital zircon U–Pb and Hf isotope analysis from the Perth Basin, Western Australia. *Gondwana Research*, *66*, 126–142.

Olierook, H. K., Jourdan, F., Merle, R. E., Timms, N. E., Kusznir, N., & Muhling, J. R. (2016). Bunbury basalt: Gondwana breakup products or earliest vestiges of the Kerguelen mantle plume? *Earth and Planetary Science Letters*, *440*, 20–32.

Olierook, H. K. H., Timms, N. E., Merle, R. E., Jourdan, F., & Wilkes, P. G. (2015). Paleodrainage and fault development in the southern Perth Basin, Western Australia during and after the breakup of Gondwana from 3D modelling of the Bunbury basalt. *Australian Journal of Earth Sciences*, *62*, 1–17.

O'Sullivan, G. J., Chew, D. M., & Samson, S. D. (2016). Detecting magma-poor orogens in the detrital record. *Geology*, *44*, 871–874.

Parra Garcia, M., Sanchez, G., Dentith, M., & George, A. (2014). *Regional structural and stratigraphic study of the Canning Basin, Western Australia*. Department of Mines and Petroleum Government of Western Australia.

Payne, J. L., Morrissey, L. J., Tucker, N. M., Roche, L. K., Szpunar, M. A., & Neroni, R. (2021). Granites and gabbros at the dawn of a coherent Australian continent. *Precambrian Research*, *359*, 106189.

Pepper, M., Gehrels, G., Pullen, A., Ibanez-Mejia, M., Ward, K. M., & Kapp, P. (2016). Magmatic history and crustal genesis of western South America: Constraints from U-Pb ages and Hf isotopes of detrital zircons in modern rivers. *Geosphere*, *12*, 1532–1555.

Prokopiev, A. V., Toro, J., Miller, E. L., & Gehrels, G. E. (2008). The paleo–Lena River—200 m.y. of transcontinental zircon transport in Siberia. *Geology*, *36*, 699.

Quentin de Gromard, R., Kirkland, C. L., Howard, H. M., Wingate, M. T., Jourdan, F., McInnes, B. I., Danišík, M., Evans, N. J., McDonald, B. J., & Smithies, R. H. (2019). When will it end? Long-lived intracontinental reactivation in central Australia. *Geoscience Frontiers*, *10*, 149–164.

Rahl, J. M., Reiners, P. W., Campbell, I. H., Nicolescu, S., & Allen, C. M. (2003). Combined single-grain (U-Th)/he and U/Pb dating of detrital zircons from the Navajo sandstone, Utah. *Geology*, *31*, 761–764.

Raimondo, T., Hand, M., & Collins, W. J. (2014). Compressional intracontinental orogens: Ancient and modern perspectives. *Earth-Science Reviews*, *130*, 128–153.

Ramsay, R. R., Eves, A. E., Denyszyn, S. W., Wingate, M., Fiorentini, M., Gwalani, L. G., & Rogers, K. A. (2019). Geology and geochronology of the Paleoproterozoic hart dolerite, Western Australia. *Precambrian Research*, *335*, 105482.

Rösel, D., Zack, T., & Boger, S. D. (2014). LA-ICP-MS U–Pb dating of detrital rutile and zircon from the Reynolds range: A window into the Palaeoproterozoic tectonosedimentary evolution of the north Australian craton. *Precambrian Research*, *255*, 381–400.

Salisbury, S. W., Romilio, A., Herne, M. C., Tucker, R. T., & Nair, J. P. (2016). The dinosaurian Ichnofauna of the lower cretaceous (Valanginian–Barremian) Broome Sandstone of the Walmadany area (James Price point), Dampier Peninsula, Western Australia. *Journal of Vertebrate Paleontology*, *36*, 1–152.

Sayers, J., Symonds, P. A., Direen, N. G., & Bernardel, G. (2001). Nature of the continent-ocean transition on the non-volcanic rifted margin of the central great Australian bight. *Geological Society, London, Special Publications*, *187*, 51–76.

Sircombe, K. N., & Freeman, M. J. (1999). Provenance of detrital zircons on the Western Australia coastline—Implications for the geologic history of the Perth basin and denudation of the Yilgarn Craton. *Geology*, *27*, 879–882.

Smith, J. (2001). Summary of results. Joint NTGS – AGSO age determination program 1999–2001. Northern Territory Geological Survey, Record 2001-007. Northern Territory Geological Survey.

Smith, T. E., Edwards, D. S., Kelman, A. P., Laurie, J. R., Le Poidevin, S. R., Nicoll, R. S., Mory, A. J., Haines, P. W., & Hocking, R. M. (2013). Canning Basin biozonation and stratigraphy, 2013, Chart 31. Geoscience Australia. http://pid.geoscience.gov.au/dataset/ga/76879

Smithies, R. H., Kirkland, C. L., Korhonen, F. J., Aitken, A., Howard, H. M., Maier, W. D., Wingate, M., Quentin de Gromard, R., & Gessner, K. (2015). The Mesoproterozoic thermal evolution of the Musgrave Province in Central Australia — Plume vs. the geological record. *Gondwana Research*, *27*, 1419–1429.

Smye, A. J., Marsh, J. H., Vermeesch, P., Garber, J. M., & Stockli, D. F. (2018). Applications and limitations of U-Pb thermochronology to middle and lower crustal thermal histories. *Chemical Geology*, *494*, 1–18.

Söderlund, U., Patchett, P., Vervoort, J. D., & Isachsen, C. E. (2004). The ^{176}Lu decay constant determined by Lu–Hf and U–Pb isotope systematics of Precambrian mafic intrusions. *Earth and Planetary Science Letters*, *219*, 311–324.

Song, Y., Ren, J., Liu, K., Lyu, D., Feng, X., Liu, Y., & Stepashko, A. (2022). Syn-rift to post-rift tectonic transition and drainage reorganization in continental rifting basins: Detrital zircon analysis from the songliao basin, China. *Geoscience Frontiers*, *13*, 101377.

Spaggiari, C. V., Kirkland, C. L., Smithies, R. H., Wingate, M., & Belousova, E. A. (2015). Transformation of an Archean craton margin during Proterozoic basin formation and magmatism: The Albany–Fraser Orogen, Western Australia. *Precambrian Research*, *266*, 440–466.

Spencer, C. J., Kirkland, C. L., & Roberts, N. M. W. (2018). Implications of erosion and bedrock composition on zircon fertility: Examples from South America and Western Australia. *Terra Nova*, *30*, 289–295.

Sundell, K., Saylor, J. E., & Pecha, M. (2019). Provenance and recycling of detrital zircons from Cenozoic Altiplano strata and the crustal evolution of western South America from combined U-Pb and Lu-Hf isotopic analysis. In B. K. Horton & A. Folguera (Eds.), *Andean tectonics: Amsterdam* (pp. 363–397). Elsevier.

Sundell, K. E., & Saylor, J. E. (2021). Two-dimensional quantitative comparison of density distributions in detrital geochronology and geochemistry. *Geochemistry, Geophysics, Geosystems*, *22*, e2020GC009559.

Thomas, M. C. (2012). *Erskine sandstone formation: A provenance and geochronological study within the Fitzroy trough, Western Australia: BSc(honours)* (p. 76). University of Adelaide.

Tomkins, H. S., Powell, R., & Ellis, D. J. (2007). The pressure dependence of the zirconium-in-rutile thermometer. *Journal of Metamorphic Geology*, *25*, 703–713.

Totterdell, J.M., Cook, P.J., Bradshaw, M.T., Wilford, G.E., Yeates, A.N., Yeung, M., Truswell, E.M., Brakel, A.T., Isem, A.R., Olissoff, S., Strusz, D.L., Langford, R.P., Walley, A.M., Mulholland, S.M., and Beynon, R.M., 2001, *Palaeogeographic Atlas of Australia*. Geoscience Australia.

Trail, D., Bruce Watson, E., & Tailby, N. D. (2012). Ce and Eu anomalies in zircon as proxies for the oxidation state of magmas. *Geochimica et Cosmochimica Acta*, *97*, 70–87.

Triebold, S., Luvizotto, G. L., Tolosana-Delgado, R., Zack, T., & von Eynatten, H. (2011). Discrimination of TiO_2 polymorphs in sedimentary and metamorphic rocks. *Contributions to Mineralogy and Petrology*, *161*, 581–596.

Triebold, S., von Eynatten, H., & Zack, T. (2012). A recipe for the use of rutile in sedimentary provenance analysis. *Sedimentary Geology*, *282*, 268–275.

Tucker, N. M., Morrissey, L. J., Payne, J. L., & Szpunar, M. (2018). Genesis of the Archean–Paleoproterozoic Tabletop domain, Rudall Province, and its endemic relationship to the West Australian Craton. *Australian Journal of Earth Sciences*, *65*, 739–768.

Tyler, I. M., Hocking, R. M., & Haines, P. W. (2012). Geological evolution of the Kimberley region of Western Australia. *Episodes*, *35*, 298–306.

Tyrrell, S., Haughton, P., & Daly, J. S. (2007). Drainage reorganization during breakup of Pangea revealed by in-situ Pb isotopic analysis of detrital K-feldspar. *Geology*, *35*, 971.

Tyrrell, S., Leleu, S., Souders, A. K., Haughton, P. D., & Daly, J. S. (2009). K-feldspar sand-grain provenance in the Triassic, west

of Shetland: Distinguishing first-cycle and recycled sediment sources? *Geological Journal*, *44*, 692–710.

Ustaömer, T., Ustaömer, P. A., Robertson, A. H. F., & Gerdes, A. (2016). Implications of U–Pb and Lu–Hf isotopic analysis of detrital zircons for the depositional age, provenance and tectonic setting of the Permian–Triassic Palaeotethyan Karakaya complex, NW Turkey. *International Journal of Earth Sciences*, *105*, 7–38.

Veevers, J. J. (2018). Gamburtsev Subglacial Mountains: Age and composition from morainal clasts and U–Pb and Hf-isotopic analysis of detrital zircons in the Lambert rift, and potential provenance of east Gondwanaland sediments. *Earth-Science Reviews*, *180*, 206–257.

Veevers, J. J., Saeed, A., Belousova, E. A., & Griffin, W. L. (2005). U–Pb ages and source composition by Hf-isotope and trace-element analysis of detrital zircons in Permian sandstone and modern sand from southwestern Australia and a review of the paleogeographical and denudational history of the Yilgarn Craton. *Earth-Science Reviews*, *68*, 245–279.

Verdel, C., Campbell, M. J., & Allen, C. M. (2021). Detrital zircon petrochronology of Central Australia, and implications for the secular record of zircon trace element composition. *Geosphere*, *17*, 538–560.

Vermeesch, P. (2018). IsoplotR: A free and open toolbox for geochronology. *Geoscience Frontiers*, *v. 9*, 1479–1493.

Vermeesch, P. (2021). On the treatment of discordant detrital zircon U–Pb data. *Geochronology*, *v. 3*, 247–257.

von Eynatten, H., & Dunkl, I. (2012). Assessing the sediment factory: The role of single grain analysis. *Earth-Science Reviews*, *115*, 97–120.

Wade, B. P., Barovich, K. M., Hand, M., Scrimgeour, I. R., & Close, D. F. (2006). Evidence for early Mesoproterozoic arc magmatism in the Musgrave block, Central Australia: Implications for Proterozoic crustal growth and tectonic reconstructions of Australia. *The Journal of Geology*, *114*, 43–63.

Walsh, A. K., Raimondo, T., Kelsey, D. E., Hand, M., Pfitzner, H. L., & Clark, C. (2013). Duration of high-pressure metamorphism and cooling during the intraplate Petermann orogeny. *Gondwana Research*, *24*, 969–983.

Watson, E. B., Wark, D. A., & Thomas, J. B. (2006). Crystallization thermometers for zircon and rutile. *Contributions to Mineralogy and Petrology*, *151*, 413–433.

Wohl, E. E., Fuertsch, S. J., & Baker, V. R. (1994). Sedimentary records of late Holocene floods along the Fitzroy and Margaret Rivers, Western Australia. *Australian Journal of Earth Sciences*, *41*, 273–280.

Xu, J., Stockli, D. F., & Snedden, J. W. (2017). Enhanced provenance interpretation using combined U–Pb and (U–Th)/he double dating of detrital zircon grains from lower Miocene strata, proximal Gulf of Mexico Basin, North America. *Earth and Planetary Science Letters*, *475*, 44–57.

Zack, T., Stockli, D. F., Luvizotto, G. L., Barth, M. G., Belousova, E., Wolfe, M. R., & Hinton, R. W. (2011). In situ U–Pb rutile dating by LA-ICP-MS: 208Pb correction and prospects for geological applications. *Contributions to Mineralogy and Petrology*, *162*, 515–530.

Zhang, J. X., Mattinson, C. G., Yu, S. Y., & Li, Y. S. (2014). Combined rutile–zircon thermometry and U–Pb geochronology: New constraints on early Paleozoic HP/UHT granulite in the south Altyn Tagh, North Tibet, China. *Lithos*, *200-201*, 241–257.

Zhang, P., Najman, Y., Mei, L., Millar, I., Sobel, E. R., Carter, A., Barfod, D., Dhuime, B., Garzanti, E., Govin, G., Vezzoli, G., & Hu, X. (2019). Palaeodrainage evolution of the large rivers of East Asia, and Himalayan-Tibet tectonics. *Earth-Science Reviews*, *192*, 601–630.

Zhang, Z., Tyrrell, S., Li, C., Daly, J. S., Sun, X., & Li, Q. (2014). Pb isotope compositions of detrital K-feldspar grains in the upper-middle Yangtze River system: Implications for sediment provenance and drainage evolution. *Geochemistry, Geophysics, Geosystems*, *15*, 2765–2779.

Zimmermann, S., Mark, C., Chew, D., & Voice, P. J. (2018). Maximising data and precision from detrital zircon U-Pb analysis by LA-ICPMS: The use of core-rim ages and the single-analysis concordia age. *Sedimentary Geology*, *375*, 5–13.

Zutterkirch, I. C., Kirkland, C. L., Barham, M., & Elders, C. (2021). Thin-section detrital zircon geochronology mitigates bias in provenance investigations. *Journal of the Geological Society*, *179*, jgs2021-070.

SUPPORTING INFORMATION

Additional supporting information can be found online in the Supporting Information section at the end of this article.

How to cite this article: Dröllner, M., Barham, M., & Kirkland, C. L. (2023). Reorganization of continent-scale sediment routing based on detrital zircon and rutile multi-proxy analysis. *Basin Research*, *35*, 363–386. https://doi.org/10.1111/bre.12715